UNIVERSITATEA BABEŞ-BOLYAI
BABEŞ-BOLYAI TUDOMÁNYEGYETEM
BABEŞ-BOLYAI UNIVERSITÄT
BABEŞ-BOLYAI UNIVERSITY
TRADITIO ET EXCELLENTIA

Babeș-Bolyai University, Cluj-Napoca, Romania
Faculty of Chemistry and Chemical Engineering
Department of Chemistry Supramolecular Organic and Organometallic Chemistry Centre

Hypercoordinated organopnictogen(III) (Sb, Bi) compounds − structure and reactivity −

PhD Thesis Abstract

Gabriel-Iulian Duneș

Scientific advisor
Prof. Dr. Cristian Silvestru

Cluj-Napoca
2022

Review committee

PRESIDENT

Prof. Dr. Ion GROSU

Babeș-Bolyai University, Cluj-Napoca, Romania

SCIENTIFIC ADVISOR

Prof. Dr. Cristian SILVESTRU

Babeș-Bolyai University, Cluj-Napoca, Romania

REVIEWERS

Dr. Yann SARAZIN

Institut de Sciences Chimiques de Rennes, UMR 6226 CNRS

Université de Rennes 1, Rennes, France

Conf. Dr. Augustin MĂDĂLAN

University of Bucharest, Bucharest, Romania

Conf. Dr. Ciprian-Ionuț RAȚ

Babeș-Bolyai University, Cluj-Napoca, Romania

Contents

Keywords: organometallic chemistry, organopnictogen, hypercoordination, NCN-pincer ligand, chalcogen, C−H bond activation

Contents of the Abstract

Keywords: organometallic chemistry, organopnictogen, hypercoordination, NCN-pincer ligand, chalcogen, C−H bond activation

I. Introduction

Since the seminal work by Moulton and Shaw[1] and by van Koten *et al.*,[2] the chemistry of pincer ligands has been expanding to various applications. The pincer ligands proved to be versatile synthons for transition metals, often used to manoeuvre between different properties at the metal centre due to a particular mixture of stability and reactivity which enabled great opportunities for various catalysts design.[3-5] The word "pincer" is derived from the Dutch word *tang* that refers to the common hardware tool known as spanner and it was coined in this regard by van Koten in 1989.[6] The ability to easily vary the type of donor atoms, the appended group at either the donor atom or within the ligated metallocycles, and to incorporate substituents remote to the metal centre allows for a high level of control of the environment around the metal. Over the past decade, the interest in hypervalent derivatives of main group metal elements increased as result of their structural peculiarities and surprisingly amenability to emulate transition-metal-like behaviour such as accessible variable oxidation states or small molecules activation.[7-9] The use of pincer-type ligands enabled the formation of hypercoordinated organo-main-group compounds. According to Muscher's and later to Perkins' formalism, hypervalent compounds of main group atoms can be designed using the *N–M–L* nomenclature, where *N* represents the number of formal valence shell electrons about the metal (*M*) that is directly bound with a number of ligands (*L*).[10-12]

While C−H bond activation reactions have classically been a domain of late transition metal chemistry, main group compounds have also successfully entered this field of research in recent years. Several examples include the activation of C−H bond in aryl, allylic, and benzylic positions and in *α*-positions of cyclic thio-ethers.[13-15] The selective activation of relatively inert C−H bonds is increasingly important in organic and organometallic synthesis, catalysis, and industrial processes because it enables efficient alternatives to multistep protocols that make use of a larger number of more conventional synthesis procedures.[16] One of the main interest in this particular research was motivated by the role of bismuth as one component in the heterogeneous "*n*MnO_3/Bi_2O_3" catalyst of the industrial SOHIO process, which is using for the large production of acrolein and acrylonitrile by allowing the oxidation and ammoxidation of propene, *i.e.* SOHIO = standard oil of Ohio.[17]

II. Original contributions

Overview

This chapter presents the original work brought to the chemistry of organopnictogen compounds during our pursuit of expanding the canonical knowledge of the coordination chemistry of antimony and bismuth. In this context the research of the presenting doctoral studies was mainly focused on exploitation of the lability of pnictogen−oxygen and pnictogen−sulfur bonds. The presenting results were divided in four main subchapters as follows.

Monoorganopnictogen(III) chlorides

This subchapter describes the synthesis and structural characterisation of a family of new organoantimony(III) and -bismuth(III) dichlorides containing different *NCN*-aryl ligands, obtained by using improved synthetic protocols. Compounds of this class were further used as useful "synthons" in reactions with different potassium aryloxides and arylthiolates.

Organopnictogen(III) bis(arylthiolates)

This subchapter presents the syntheses of a series of new well-defined hypercoordinated organopnictogen(III) thiolates and the study of the propensity of these complexes to undergo a reductive elimination process and to generate stable four-membered organometallic heterocycles upon reaction with chalcogens.

Organopnictogen(III) bis(aryloxides)

Compounds of this class are mainly used as precursors for the synthesis of metal oxide-containing materials prepared by the CVD process (chemical vapor deposition). Seldom examples of monoorganopnictogen(III) aryloxides are known to date and herein three new pnictogen(III) aryloxides characterised in solution and in the solid state are reported.

Pnictogen-mediated C−H bond activation. Pnictogen (Sb, Bi) *NCN* pincer complexes with the oxyaryl dianionic ligand, $(C_6H_2{}^tBu_2\text{-}3,5\text{-}O\text{-}4)^{2-}$.

This subchapter describes the syntheses of the unique oxyaryl antimony and bismuth complexes formed by C−H bond activation and their structural peculiarities. DFT calculations were undertaken for the proposed mechanism.

II.I. Monoorganopnictogen(III) chlorides

The organopnictogen(III) precursors [2,6-{O(CH$_2$CH$_2$)$_2$NCH$_2$}$_2$C$_6$H$_3$]PnCl$_2$ [Pn = Sb (**1**), Bi (**2**)] were prepared by the lithiation of the proligand 2,6-{O(CH$_2$CH$_2$)$_2$NCH$_2$}$_2$C$_6$H$_3$Br with a slight excess of ^{n}BuLi, in hexane at room temperature, under argon atmosphere. An improved method was further developed to obtain the title compounds **1** and **2** in higher yields, 63% and 65%, respectively, in this endeavour the organolithium compound [2,6-{O(CH$_2$CH$_2$)$_2$NCH$_2$}$_2$C$_6$H$_3$]Li was generated *in situ* at −78 ºC, in THF and was further reacted with 1 equivalent of PnCl$_3$ [Pn = Sb, Bi] in THF, at −78 ºC (Scheme 1).

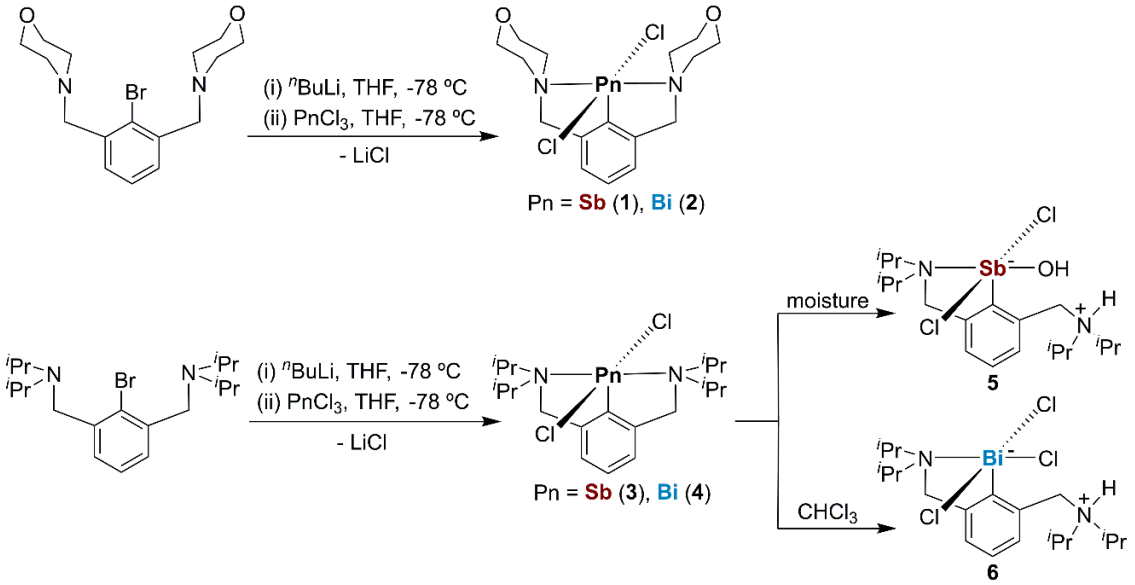

Scheme 1. Syntheses of compounds **1**−**4**.

The later synthetic protocol was used to prepare the analogues arylpnictogen dichlorides [2,6-(^{i}Pr$_2$NCH$_2$)$_2$C$_6$H$_3$]PnCl$_2$ [Pn = Sb (**3**), Bi (**4**)] (Scheme 10) following the initial lithiation of the 2,6-(^{i}Pr$_2$NCH$_2$)$_2$C$_6$H$_3$Br as described for the tin analogue [2,6-(^{i}Pr$_2$NCH$_2$)$_2$C$_6$H$_3$]SnCl.[18] The organic proligands 2,6-{O(CH$_2$CH$_2$)$_2$NCH$_2$}$_2$C$_6$H$_3$Br[19] and 2,6-(^{i}Pr$_2$NCH$_2$)$_2$C$_6$H$_3$Br[20] were synthesised according to the literature procedures. Compounds **3** and **4** were isolated as pale-yellow solids.

All the discussed compounds were investigated in solution by NMR spectroscopy and the unambiguous assignment of the ^{1}H and ^{13}C{^{1}H} NMR resonance signals was carried out based on COSY, HSQC and HMBC correlation experiments. The numbering scheme used for the assignment of the resonance signals (^{1}H and ^{13}C{^{1}H} NMR) for compounds **1** and **2** is shown in Scheme 2.

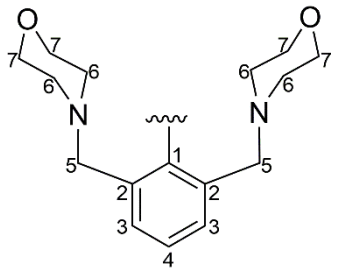

Scheme 2. Numbering scheme of the ligand 2,6-{$O(CH_2CH_2)_2NCH_2\}_2C_6H_3$ used in NMR assignments.

The ^{1}H and $^{13}C\{^{1}H\}$ NMR spectra of **1** and **2** exhibited only one set of resonance signals in the alkyl region which indicates the equivalence of the two pendant amines. The observed behaviour of **1** and **2** (Figure 1) in solution is consistent with other related organopnictogen(III) dihalides,[21,22] and is indicative of a strong N→Pn interaction, as observed in the solid state (*vide infra*), which restricts the *vertex* inversion at the nitrogen atoms and the conformational inversion of the morpholinyl rings. Hence, there are four type of protons designated as H_{6a}, H_{6e}, H_{7a} and H_{7e}, considering their relative positions to the morpholinyl ring and the N→Pn bond

Noteworthy, the $^{13}C\{^{1}H\}$ NMR spectra of compounds **1** and **2** showed similar feature, namely the most down-field shifted resonances correspond to the *ipso* carbon atoms (directly bonded to the metal centre) at δ_{Cq} 152.07 ppm for **1** and δ_{Cq} 204.78 ppm for **2**, respectively. The remarkably deshielded position of the signal assigned to the *ipso*-carbon bonded to bismuth in **2** (and generally in all the Bi(III) compounds presented in this work) compared to the analogue signal corresponding to the carbon atom bonded to antimony in **1**, can be attributed mostly to the spin-orbital heavy-atom effect on the light atom (SO-HALA effect).[23]

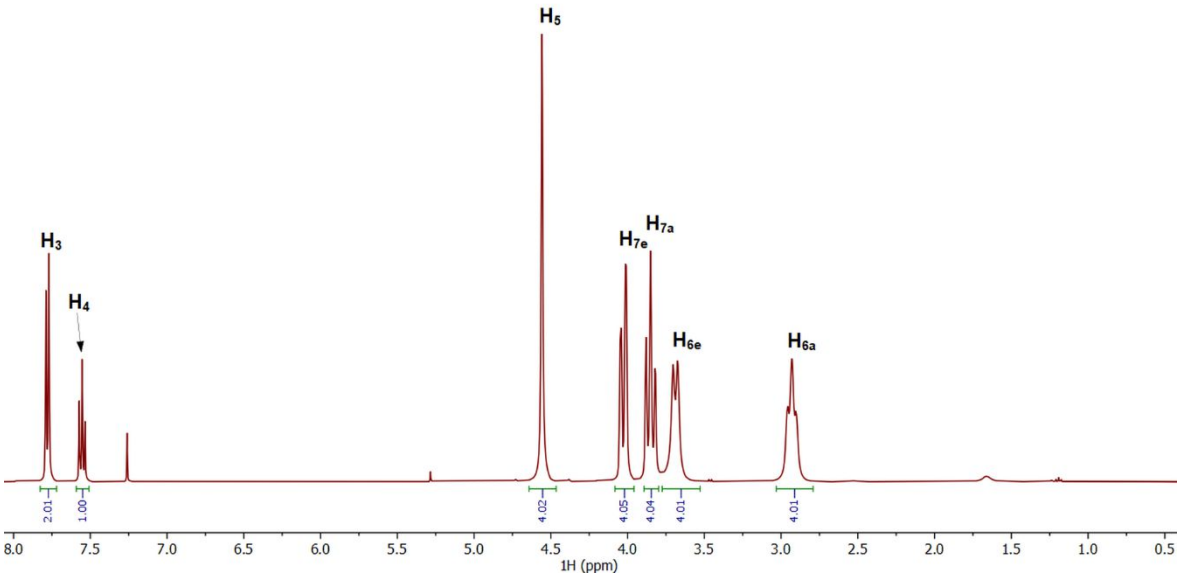

Figure 1. ^{1}H NMR ($CDCl_3$, 400.13 MHz) spectrum of [2,6-{$O(CH_2CH_2)_2NCH_2$}$_2C_6H_3$]$BiCl_2$ (**2**) at r.t.

The molecular structure of **1** exhibits a T-shaped $CSbX_2$ core (X = Cl/Br), with chlorine atoms placed in *trans* positions [Cl1−Sb1−Cl2 171.65(12)°], *i.e.* the presence of residual bromine atoms will be neglected in the following discussion of the molecular structure (Figure 2). The *trans* Sb−Cl bond distances in compound **1** are considerably longer [Sb1−Cl1 2.700(7) Å; Sb1−Cl2 2.608(4) Å] than the sum of covalent radii of the corresponding atoms [Σr_{cov}(Sb,Cl) 2.41 Å],[24] which is in agreement with the 3c-4e theory of the hypervalent bond formation. Nitrogen atoms from both pendant arms of the *NCN*-aryl pincer ligand coordinate strongly to the antimony centre in a *meridional* fashion [N1−Sb1−N2 151.07(9)°], as demonstrated by the corresponding intramolecular Sb−N distances [Sb1−N1 2.471(3) Å; Sb2−N2 2.480(3) Å] [*cf.* Σr_{cov}(Sb,N) 2.10 Å,[24] and Σr_{vdW}(Sb,N) 4.13 Å,[25] respectively].

As a result of the *NCN* scaffold behaviour the overall coordination geometry at antimony in **1** is best described as distorted square pyramidal with τ_5 = 0.34 (τ_5 = 1.00 for ideal trigonal bipyramidal structure and 0.00 for square-based pyramidal geometries)[26] and with the carbon atom located in the apical position of the (*NCN*)$SbCl_2$ core (hypervalent *12-Sb-5* species).[11]

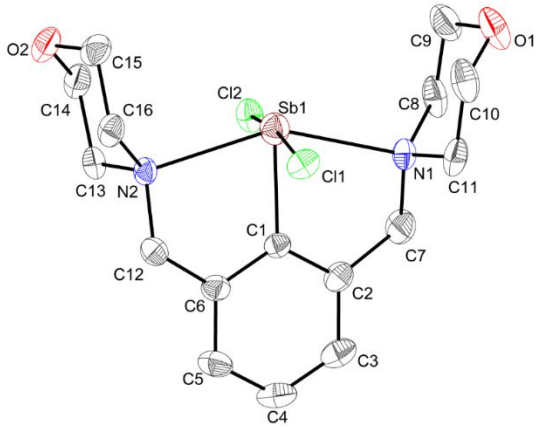

Figure 2. ORTEP representation of the isomer (pR$_{N1}$,pR$_{N2}$)-**1** with ellipsoids drawn at the 50% probability level, present in the crystal of **1**·CHCl$_3$. Hydrogen atoms were omitted for clarity.

The molecular structure of compound **2** (Figure 3) bears a close resemblance to that of **4** (Figure 3) and exhibits some common features at the molecular level such as: (*i*) the primary coordination sphere consists of a T-shaped CBiCl$_2$ core, with *trans* chlorine atoms [**2**: Cl1−Bi1−Cl2 173.80(2)°; **4**: Cl1−Bi1−Cl1a 175.50(1)°] as reported for the related monoorganobismuth(III) halides [2,6-(Me$_2$NCH$_2$)$_2$C$_6$H$_3$]BiX$_2$ [X = Cl, Br, I][27] and [2,6-{MeN(CH$_2$CH$_2$)$_2$NCH$_2$}$_2$C$_6$H$_3$]BiX$_2$ [X = Cl, Br, I][22]; (*ii*) each CBiCl$_2$ core is strongly coordinated by the *NCN* pincer ligand *trans* to each other through nitrogen atoms from both pendant arms [**2**: Bi1−N1 2.561(2), Bi1−N2 2.565(2) Å; **4**: Bi1−N1 2.615(2), Bi1−N1a 2.615(2) Å] [*cf.* the sum of the covalent and the van der Waals radii Σr_{cov}(Bi,N) 2.19 Å,[24] Σr_{vdW}(Bi,N) 4.20 Å[25]]; (*iii*) taking into account the intramolecular N→Bi interactions the resulting overall geometry around bismuth is distorted square pyramidal (τ_5 = 0.47 for **2** and τ_5 = 0.42 for **4**).[26]

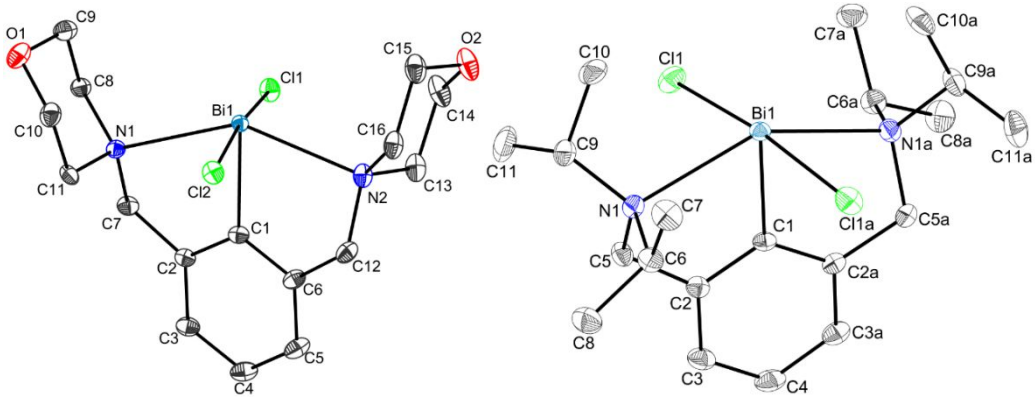

Figure 3. ORTEP representation of isomers (pR$_{N1}$,pR$_{N2}$)-**2** (left) and (pR$_{N1}$,pR$_{N1a}$)-**4** (right) with ellipsoids drawn at the 50% probability level, present in the crystal of **1**·CHCl$_3$ and **4**, respectively [symmetry equivalent atoms (*1-x, 1-y, z*) are given by "a"]. Hydrogen atoms were omitted for clarity.

Several attempts of crystallisation of compound **3** from a concentrated acetonitrile solution of the title compound failed, instead yielded single crystals of **5**·CH_3CN of quality appropriate for X-ray diffraction analysis. The molecule of **5** (Figure 4) consists of a five-coordinate structure where the coordination geometry about antimony is distorted square-based pyramidal with $\tau_5 = 0.05$ ($\tau_5 = 1.00$ for ideal trigonal bipyramidal and 0.00 for square pyramidal geometries).[26] The potentially tridentate *NCN*-aryl ligand acts as a *CN*-chelating ligand, *i.e.* only one out of the two potential pendant arms is coordinated to the Sb centre [Sb1−N1 2.953(1) Å], the other is not interacting with the antimony centre as a result of the protonated pendant amine [N2−H2 0.886(1) Å, *cf.* Σr_{cov}(N,H) 1.02 Å[24]].

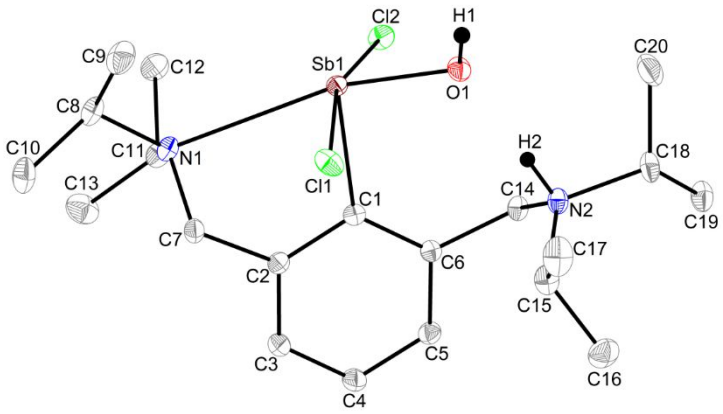

Figure 4. ORTEP representation of the zwitterion (pS_{N1})-[2-(^{i}Pr$_2$NCH$_2$)-6-{^{i}Pr$_2$N$^+$(H)CH$_2$}C$_6$H$_3$]Sb$^-$Cl$_2$(OH) (**5**·CH_3CN) with ellipsoids drawn at the 50% probability level. Hydrogen atoms except H1 and H2, the (pR_{N1})-**5** isomer presented in the unit cell and the CH_3CN solvent molecule were omitted for clarity.

II.II. Organopnictogen(III) bis(arylthiolates)

The anticipated bis(arylthiolates) [2,6-(Me_2NCH_2)$_2$$C_6H_3$]Sb($SC_6H_3Me_2$-2,6)$_2$ (**7**) and [2,6-(Me_2NCH_2)$_2$$C_6H_3$]Bi($SC_6H_3Me_2$-2,6)$_2$ (**8**) were obtained, in high yields, by reacting the previously reported arylpnictogen dichlorides, R^1PnCl_2 [R^1 = 2,6-(Me_2NCH_2)$_2$$C_6H_3$; Pn = Sb,[24a] Bi[50]] with 2 equivalents of $KSC_6H_3Me_2$-2,6 and were isolated as air sensitive yellow and dark orange solids, respectively (Scheme 3).

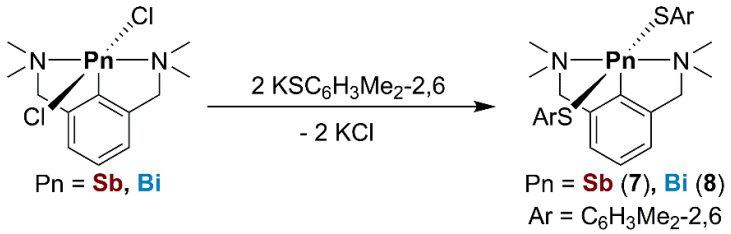

Scheme 3. Syntheses of pnictogen thiolates **7** and **8**.

Different organopnictogen(III) precursors containing bulkier *NCN*-pincer scaffold akin to 2,6-(Me_2NCH_2)$_2$$C_6H_3$ were further used, *i.e.* R^2PnCl_2 [R^2 = 2,6-{$MeN(CH_2CH_2)_2NCH_2$}$_2$$C_6H_3$; Pn = Sb,[21] Bi[22]] and R^3PnCl_2 [R^3 = 2,6-{$O(CH_2CH_2)_2NCH_2$}$_2$$C_6H_3$; Pn = Sb (**1**), Bi (**2**)].

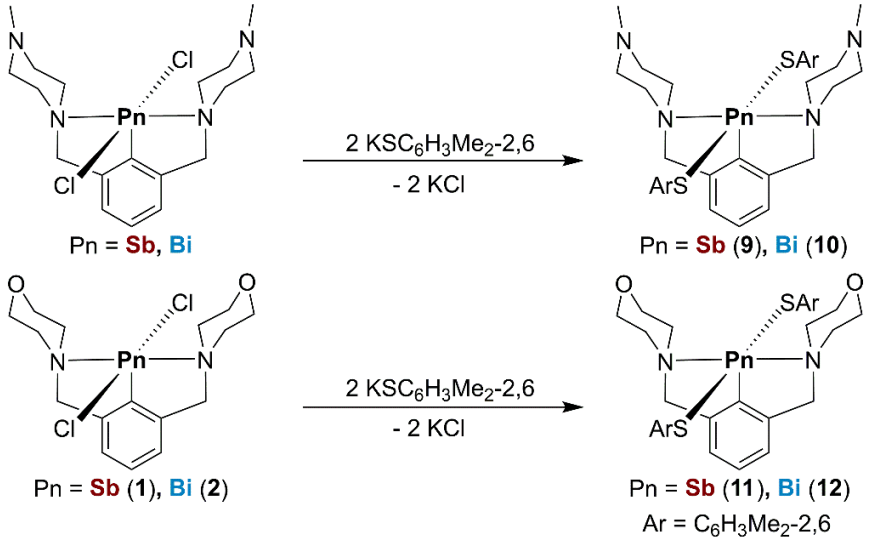

Scheme 4. Syntheses of pnictogen thiolates **9**–**12**.

In this endeavour, similarly to **7** and **8**, the new monoorganopnictogen(III) bis(arylthiolates) [2,6-{$MeN(CH_2CH_2)_2NCH_2$}$_2$$C_6H_3$]Pn($SC_6H_3Me_2$-2,6)$_2$ [Pn = Sb (**9**), Bi (**10**)] and [2,6-{$O(CH_2CH_2)_2NCH_2$}$_2$$C_6H_3$]Pn($SC_6H_3Me_2$-2,6)$_2$ [Pn = Sb (**11**), Bi (**12**)] were synthesised in a straightforward salt elimination reaction between the parent arylantimony(III) or -bismuth(III) chlorides and two equivalents of $KSC_6H_3Me_2$-2,6 in THF

(Scheme 4). Compounds **9**−**12** were isolated as air-sensitive yellow (**9**, **11**) and dark orange (**10**, **12**) solids, stable in inert argon atmosphere.

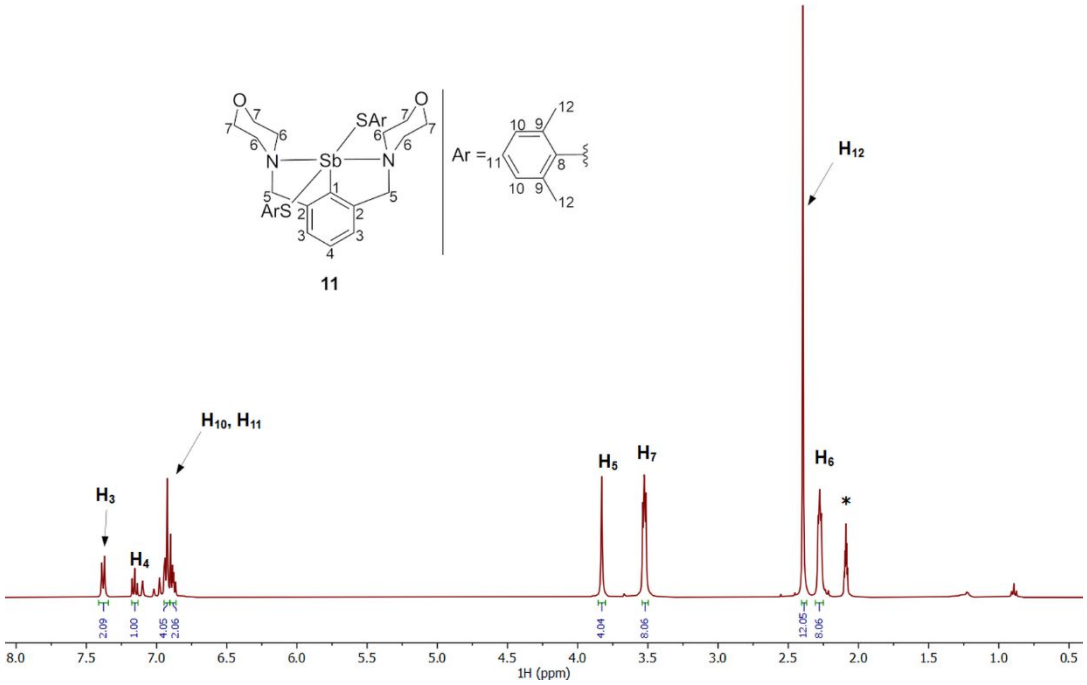

Figure 5. ^{1}H NMR (toluene-d$_8$, 400.13 MHz) spectrum of [2,6-{O(CH$_2$CH$_2$)$_2$NCH$_2$}$_2$C$_6$H$_3$]Sb(SC$_6$H$_3$Me$_2$-2,6)$_2$ (**11**) (* denotes residual protio solvent fraction of toluene-d$_8$) at r.t.

Compounds **7**−**12** are stable in solution at room temperature in dry and degassed toluene-d$_8$ or CD_2Cl_2, but fully decompose in $CDCl_3$. The methylene protons of both pendant amines exhibit broad (**9**, **11**) or sharp (**10**, **12**) singlet resonances. The broadening of the resonances noticed in the ^{1}H NMR spectra of compounds **9** and **11** (Figure 5) and especially in the case of **7** can be associated with a dynamic process which implies an alternative coordination of the pendant arms as it was later shown for the solid-state molecular structures of **7** and **11** where only one amine group is coordinated to the antimony centre (*vide infra*). In the aliphatic region of ^{1}H NMR spectra of compounds **9**−**12** the methylene protons of the NCH$_2$CH$_2$NMe and NCH$_2$CH$_2$O fragments appear as two broad multiplet resonances as a result of a fast conformational inversion combine with *vertex* inversion at the nitrogen atoms of the corresponding cycles.

The ESI+ high resolution mass spectra of **7**−**12** did not contain the protonated molecular ion [M$^+$ + H], although the most abundant peaks in the case of antimony(III) thiolates **7**, **9** and **11** correspond to the fragments [RSbOH]$^+$ [*m/z* 329.06144 (100%) for **7**;

m/z 439.14538 (100%) for **9**; *m/z* 413.07982 (53%) for **11**] and $[RSb(SAr)]^+$ [*m/z* 449.10155 (95%) for **7**; *m/z* 559.18520 (67%) for **9**; *m/z* 533.11861 (100%) for **11**]. The detection of such oxoantimony(III) fragments might suggest a decomposition pattern of the parent thiolates in the presence of H_2O or O_2. In contrast, in the ESI+ mass spectra of bismuth(III) thiolates **8**, **10** and **12**, no such oxobismuth(III) species were detected and the base peaks correspond to the $[M - SAr]^+$ fragment, *i.e.* the $[RBi(SAr)]^+$ [*m/z* 537.17734 (100%) for **8**; *m/z* 647.26587 (100%) for **10**; *m/z* 621.19448 (100%) for **12**].

Compounds **7** and **8** crystallise with two independent molecules in the asymmetric unit and one of the pendant arms in the molecular structure of **11** was found to be disordered with site occupancies of 40% (A) and 60% (B). The molecular structures of **7a**, **7b** (Figure 6) and **11**·THF (Figure 7) are noticeably similar. In all three cases only one of two pendant amines of the *NCN*-aryl ligand is coordinated to the antimony centre as suggested by the intramolecular Sb−N distances [**7a**: Sb1−N1 2.737(1) Å; **7b**: Sb2−N3 2.666(12) Å; and **11**: Sb1−N1 2.843(1) Å], which are elongated in comparison with analogues distances in the precursor R^1SbCl_2 [Sb−N 2.422(8) and 2.491(9) Å[28]], but shorter than Σr_{vdW}(Sb,N) 4.13 Å.[25]. The Sb−S bond in *trans* relative to the N→Sb interaction is directly influenced by the strength of the internal nitrogen−antimony coordination, thus the shorter the Sb−N bond is, the longer the corresponding Sb−S bond as showed by the bond pairs lengths Sb1−N1 / Sb1−S1 2.843(1) Å / 2.491(4) Å in **11** and 2.737(10) Å / 2.516(4) Å in **7a** and Sb2−N3 / Sb2−S3 2.666(12) Å / 2.519(4) Å in **7b**.

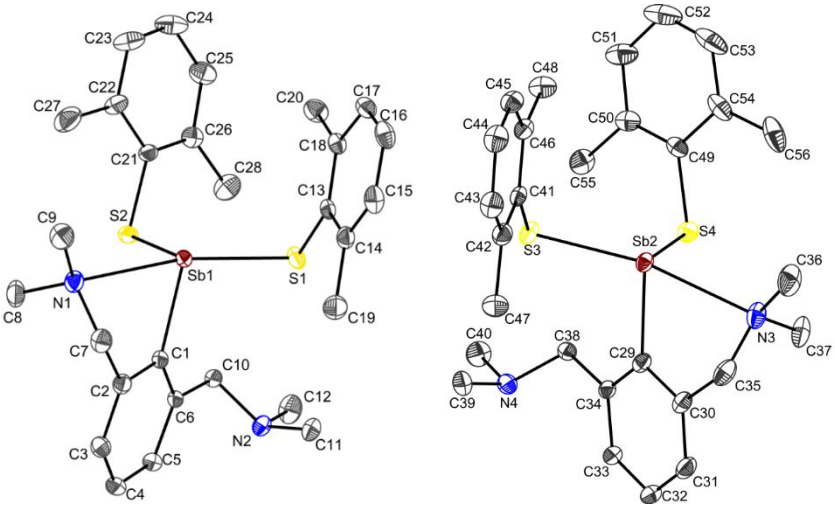

Figure 6. ORTEP representation of isomers (pS_{N1},C_{Sb1})-**7a** (left) and (pR_{N3},A_{Sb2})-**7b** (right) with ellipsoids drawn at the 50% probability level. Hydrogen atoms were omitted for clarity.

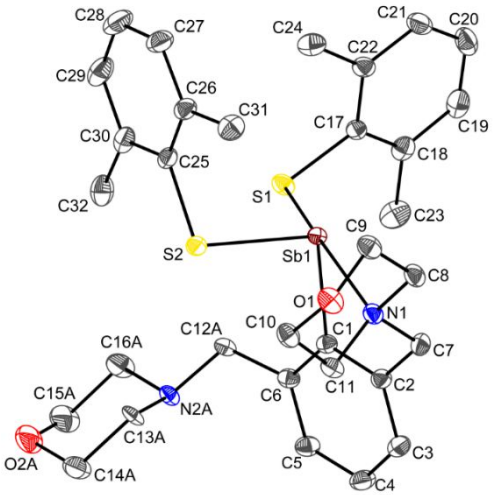

Figure 7. ORTEP representation of the isomer (pS$_{N1}$,C$_{Sb1}$)-**11** [only one site occupancy for the disordered pendant arm is depicted] with ellipsoids drawn at the 50% probability level. Hydrogen atoms were omitted for clarity.

Contrarily to the antimony thiolates **7** and **11**, the molecular structures of **8** (Figure 8) and **12** (Figure 9) revealed an *NCN*-pincer behaviour of the aryl scaffolds, namely in molecules **8a** and **8b** the pincer ligand adopts a *meridional* coordination mode [**8a**: N1−Bi1−N2 144.38(4)°; **8b**: N3−Bi2−N4 144.09(5)°] with the *ipso* carbon atoms C1 and C29, respectively, in apical positions, while the pertaining coordinative nitrogen atoms occupy *trans* basal sites in distorted square based pyramidal bismuth environments. In the case of **12** the *NCN*-aryl ligand preferred to coordinate in a *facial* fashion [N1−Bi1−N2 110.94(5)°] in *trans* to Bi−S bonds [N1−Bi1−S1 153.88(4)°; N2−Bi1−S2 150.14(4)°] as the geometry around the five-coordinate Bi atom is distorted square pyramidal with the N1 and N2 atoms placed in *cis* position in the basal plane and the C1 atom in apical position.

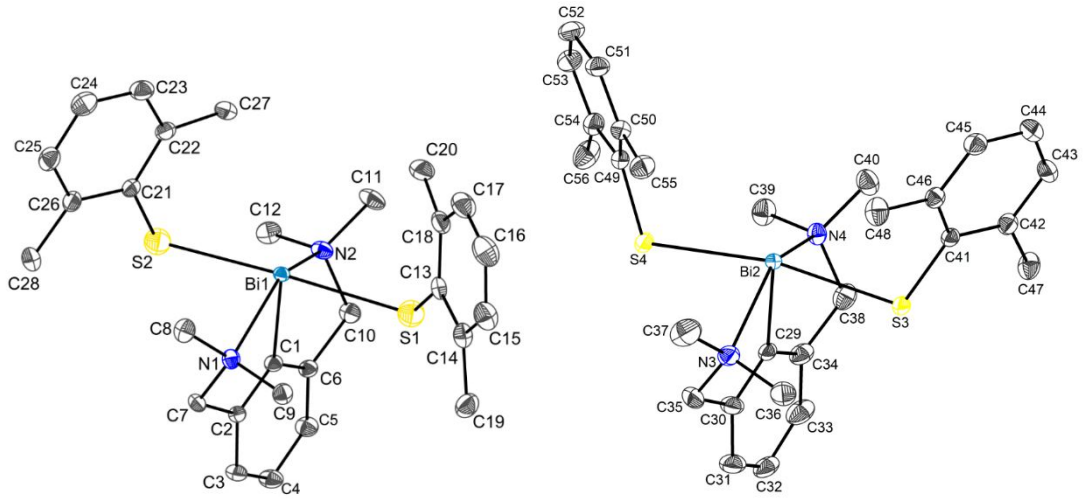

Figure 8. ORTEP representation of isomers (pR_{N1},pR_{N2})-**8a** (left) and (pR_{N3},pR_{N4})-**8b** (right) with ellipsoids drawn at the 50% probability level. Hydrogen atoms were omitted for clarity.

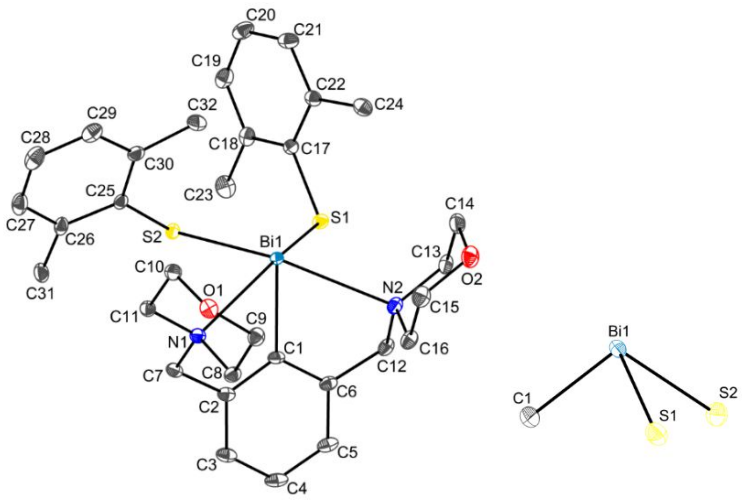

Figure 9. ORTEP representation of the isomer (pR_{N1},pS_{N2})-**12** with ellipsoids drawn at the 30% probability level. View of the pyramidal $CBiS_2$ core (right). Hydrogen atoms were omitted for clarity.

Reactions of the new organopnictogen(III) bis(thiolates) with chalcogens. Compounds **7** and **8** proved to be reluctant to hydrolysis, this behaviour being consistent with other related reports.[29] In this sense, the new organopnictogen(III) thiolates could undergo an aerobic decomposition pathway as the homoleptic antimony(III) and bismuth(III) arylthiolates $Pn(EC_6H_2R_3\text{-}2,4,6)_3$ (E = S, Se; R = Me, ^{i}Pr, ^{t}Bu) were reported to decompose in solution to the corresponding disulfides catalysed by the presence of molecular oxygen.[30]

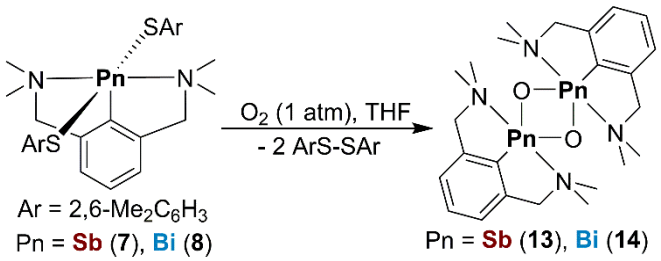

Scheme 5. Aerobic decomposition of compounds **7** and **8**.

To assess this idea, separated degassed THF solutions of compounds **7** and **8** were exposed to a dry O_2 atmosphere (1 atm) (Scheme 5). Over the course of several minutes the yellow (**7**) and the dark orange (**8**) solutions turned pale yellow.

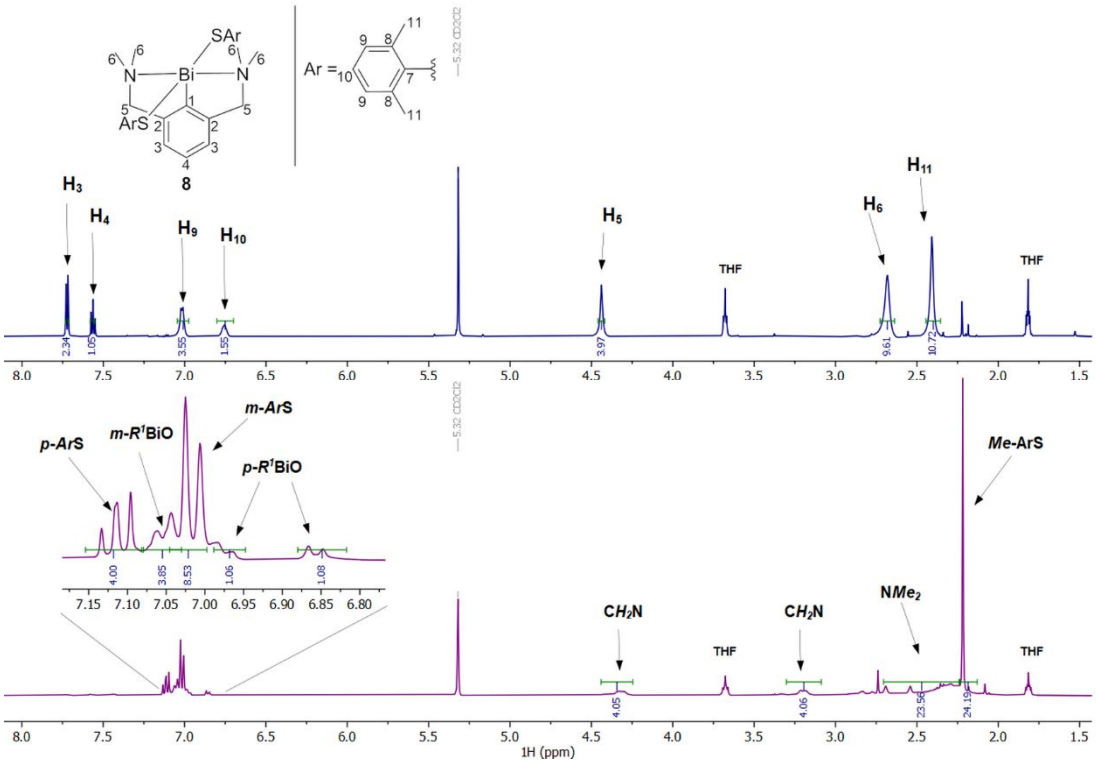

Figure 10. ^{1}H NMR (CD_2Cl_2, 400.13 MHz) spectra of [2,6-$(Me_2NCH_2)_2C_6H_3$]Bi($SC_6H_3Me_2$-2,6)$_2$ (**8**) (blue) and of the crude products formed after its aerobic decomposition within 1 h (magenta).

^{1}H NMR spectra of the resulting solutions (Figure 10) indicated the complete consumption of the title compounds and the presence of two different species, namely identified as the organic oxidation product ArS−SAr (Ar = $C_6H_3Me_2$-2,6)[31] and the known corresponding cyclic oxides *cyclo*-[2,6-$(Me_2NCH_2)_2C_6H_3Pn(\mu$-O)]$_2$ [Pn = Sb (**13**),[32] Bi(**14**),[33]], in *ca.* 2:1 ratio.

The molecular structure revealed that **14** crystallised about an inversion centre with the Bi−C bonds of the *NCN*-aryl ligands lying almost orthogonal to the planar Bi_2O_2 ring in an *anti*-orientation of the corresponding Bi−C bonds (relative to the Bi_2O_2 core), thus in the crystal of **14** only the *cyclo-anti*-(*p*R$_{N1}$,*p*S$_{N2}$)(*p*S$_{N1a}$,*p*R$_{N2a}$) isomer was observed (Figure 11). The pincer ligand 2,6-$(Me_2NCH_2)_2C_6H_3$ preferred a *cis* coordination of the pendant amine arms to the bismuth centres [N1−Bi1−N2 121.19(4)°], where each nitrogen atom coordinates almost *trans* to a Bi−O bond [N1−Bi1−O1a 146.60(4)°; N2−Bi1−O1 148.55(4)°]. As a result of this *NCN*-coordination pattern the central four-membered Bi_2O_2 core is slightly asymmetric [Bi1−O1 2.132(13) Å, Bi1−O1a 2.114(12) Å, *cf.* Σr_{cov}(Bi,O) 2.14 Å[24]] with different *endocyclic* angles [Bi1−O1−Bi1a 100.27(5)°; O1−Bi1−O1a 79.73(5)°].

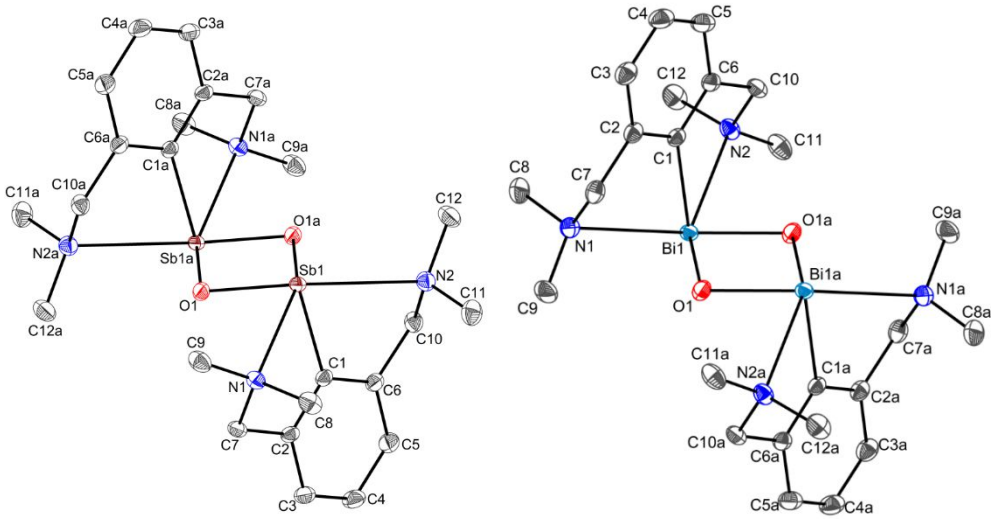

Figure 11. ORTEP representation of isomers *cyclo-anti*-(*p*R$_{N1}$,*p*S$_{N2}$)(*p*S$_{N1a}$,*p*R$_{N2a}$)-**13** (left) and *cyclo-anti*-(*p*R$_{N1}$,*p*S$_{N2}$)(*p*S$_{N1a}$,*p*R$_{N2a}$)-**14** (right) with ellipsoids drawn at the 50% probability level. Hydrogen atoms were omitted for clarity clarity [symmetry equivalent atoms (*1–x, 1–y, 1–z*) are given by "a"].

Weak interannular Bi···Bi interactions between dinuclear *anti*-(*p*R$_{N1}$,*p*S$_{N2}$)(*p*S$_{N1a}$,*p*R$_{N2a}$) units, shorter than the double of bismuth van der Waals radii [Bi1···Bi1b 4.15 Å, *cf.* Σr_{vdW}(Bi,Bi) 5.08 Å[25]] lead to the formation of a polymeric chain in the crystal of **14** (Figure 12).

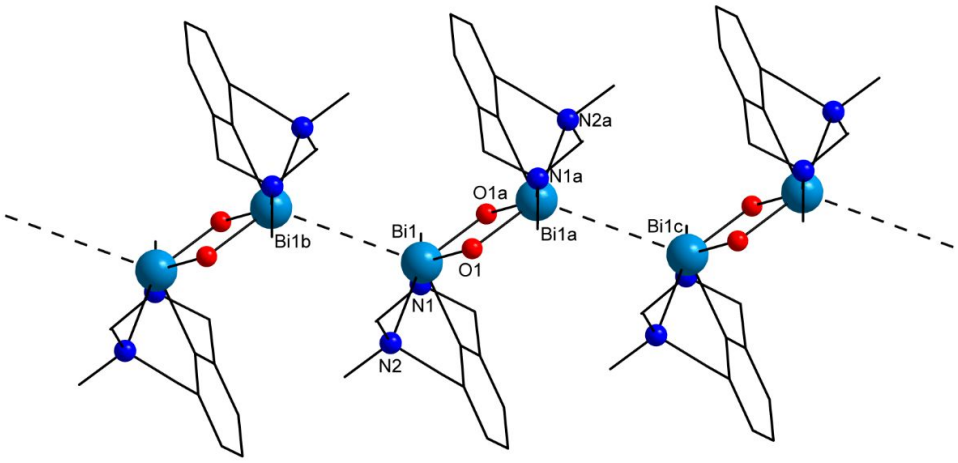

Figure 12. View along *b* axis of a polymeric chain built *via* intermolecular Bi···Bi interactions in the crystal of **14** [Symmetry transformations used to generate equivalent atoms given by "a", "b" and "c": (*1–x, 1–y, 1–z*), (*2–x, 1–y, 1–z*) and (*-1+x, y, z*), respectively].

On the whole, based on the combined experimental results, it can be envisaged a tentative mechanism (Scheme 6) where the first step is the oxidative addition of the chalcogen to the monoorganopnictogen(III) thiolate which generates elusive Pn(V) transient species, that easily eliminates the disulfide ArS−SAr through a reductive elimination process to form reactive monomeric [2,6-(Me_2NCH_2)$_2$$C_6H_3$]Pn=O species which undergo a fast [2+2] cycloaddition to the more stable cyclic dinuclear oxide, *i.e.* **13** and **14**.

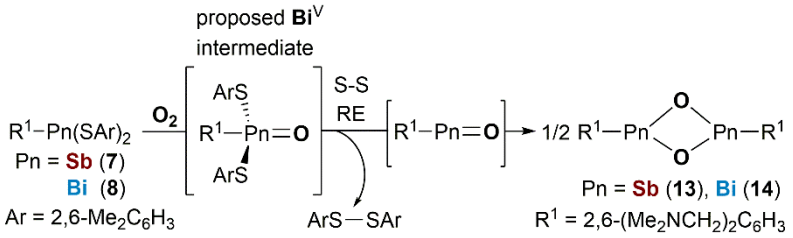

Scheme 6. A tentative mechanism for the formation of **13** and **14**.

In order to explore the observed propensity, compound **7** was mixed with a stoichiometric amount of elemental sulfur in THF (Scheme 7) and the initial bright yellow solution faded immediately. The ^{1}H and ^{13}C{^{1}H} NMR spectra of the crude mixture confirmed the presence of the disulfide ArS−SAr (Ar = $C_6H_3Me_2$-2,6)[31] and the *cyclo*-[2,6-(Me_2NCH_2)$_2$$C_6H_3$Sb($\mu$-S)]$_2$ (**15**),[34] when compared the observed data with the published ones.

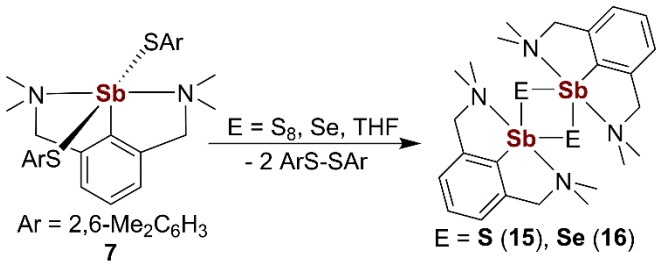

Scheme 7. Reaction of **7** with chalcogens.

Following a similar protocol the reaction of antimony thiolate **7** with Se gave the antimony selenide [2,6-(Me_2NCH_2)$_2$$C_6H_3$]Sb=Se (**16**). On a level with the solid-state structure of **14**, the diselenide **16** exhibits a slightly asymmetric central four-membered Sb_2Se_2 ring [Sb1−Se1−Sb1a 94.27(2)°; Se1−Sb1−Se1a 85.73(1)°] (Figure 13) with the Sb−Se bond distances [Sb1−Se1 2.610(5) Å; Sb1−Se1a 2.636(5) Å] closer to a normal covalent single bond [*cf.* Σr_{cov}(Sb,Se) 2.59 Å[24]], and significantly longer than the distance for the Sb=Se double bond observed in its monomeric structure [2,6-(Me_2NCH_2)$_2$$C_6H_3$]Sb=Se [Sb−Se 2.439(7) Å[35]].

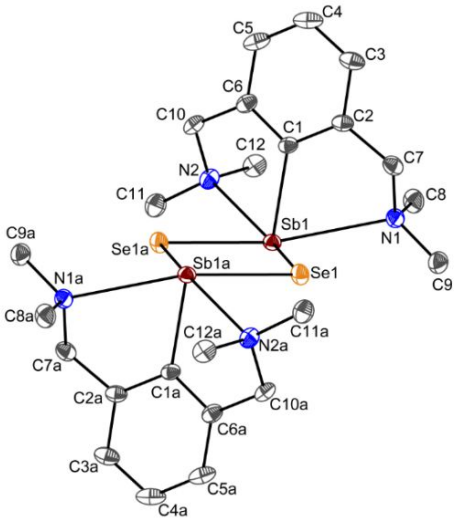

Figure 13. ORTEP representation of the isomer *cyclo-anti*-(*p*S_{N1},*p*R_{N2})(*p*R_{N1a},*p*S_{N2a})-**16** with ellipsoids drawn at the 50% probability level, present in the crystal of **16**. Hydrogen atoms were omitted for clarity[symmetry equivalent atoms (*1–x, 1–y, 1–z*) are given by "a"].

Reaction of 12 with iodine. The monoorganobismuth iodide [2,6-{O(CH$_2$CH$_2$)$_2$NCH$_2$}$_2$C$_6$H$_3$]BiI$_2$ (**17**) was isolated from the reaction of the bismuth thiolate **12** with 1 equiv of iodine in THF (Scheme 8).

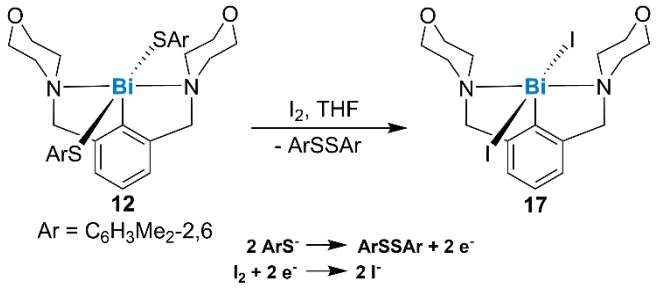

Scheme 8.

Surprisingly when 2 equivalents of iodine were added, co-crystals of **17**·0.5**I$_2$** were grown from a concentrated THF solution. The solid state molecular structure revealed a heterotrimer unit (**17**···I$_2$···**17**) which contains the (*p*S$_{N1}$,*p*S$_{N2}$)- and (*p*R$_{N1}$,*p*R$_{N2}$)-**17** isomers linked to one another through I$_2$ molecule where the diatomic iodine adopts an *end-on* bridging coordination (Figure 14). Several experimental observations were made on the basis of IUPAC definition of halogen bonding (XB),[36] where the molecules of **17** act as halogen-bond acceptors (XBAs), while the molecular iodine is a halogen-bond donor (XBD).

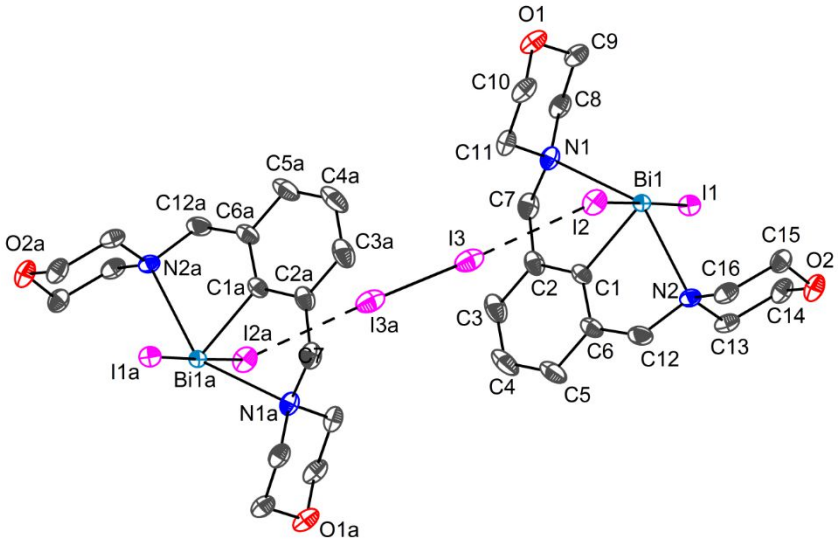

Figure 14. ORTEP representation of (**17**···I$_2$···**17**) with ellipsoids drawn at the 20% probability level. Hydrogen atoms were omitted for clarity [symmetry equivalent atoms (–*x*, 2–*y*, 1–*z*) are given by "a"].

II.III. Organopnictogen(III) bis(aryloxides)

The salt metatheses of R^1PnCl_2 [R^1 = 2,6-$(Me_2NCH_2)_2C_6H_3$; Pn = Sb, Bi], with 2 equivalents of $KOC_6H_3{}^iPr_2$-2,6 and $KOC_6H_3(OMe)_2$-2,6 (Scheme 9), in THF, lead to the formation of the novel bis(aryloxide) complexes $R^1Sb(OC_6H_3{}^iPr_2\text{-}2,6)_2$ (**18**), $R^1Sb[OC_6H_3(OMe)_2\text{-}2,6]_2$ (**19**) and $R^1Bi[OC_6H_3(OMe)_2\text{-}2,6]_2$ (**20**) as off-white (**18**, **19**) and bright yellow (**20**) solids, respectively, in high yields. Compounds **18**–**20** are air- and moisture-sensitive and should be definitely stored under inert atmosphere.

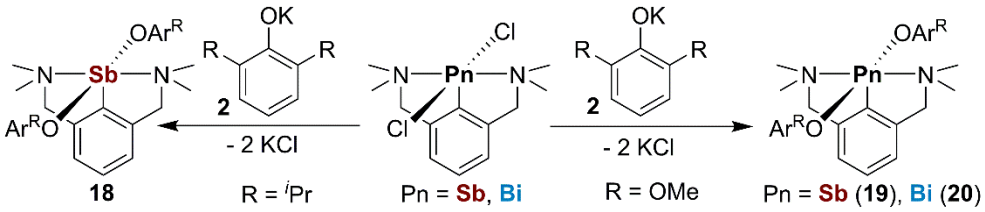

Scheme 9. Syntheses of pnictogen aryloxides **18**–**20**.

The ^1H and $^{13}C\{^1H\}$ NMR spectra of compounds **18**–**20** are consistent with molecular C_{4v} symmetry, *i.e.* only one set of resonances for the R^1 protons and OAr [Ar = $C_6H_3{}^iPr_2$-2,6 or $C_6H_3(OMe)_2$-2,6] groups were observed in the NMR spectra. The ^1H NMR spectra of **18**–**20** recorded in C_6D_6 for **18** and **20** and in CD_3CN for **19**, exhibit a common feature of the R^1 scaffold, *i.e.* two broad singlet signals for the methyl and methylene groups, respectively.

The molecular structures of compounds **18** and **20** were established by X-ray diffraction analysis of suitable single crystals and are depicted in Figure 15 and Figure 16, respectively. The solid-state structure of **18** features a T-shaped $CSbO_2$ core, with oxygen atoms placed mutually in *trans* position [O1–Sb1–O1a 165.72(6)°] and with the *NCN* scaffold coordinated to the metal centre through the nitrogen atoms of both pendant arms in a *meridional* fashion [N1–Sb1–N1a 149.31(6)°]. This *NCN*-pincer behaviour results in the formation of a hypervalent *12-Sb-5* species,[11] with an overall distorted square pyramidal (*NCN*)SbO_2 core.

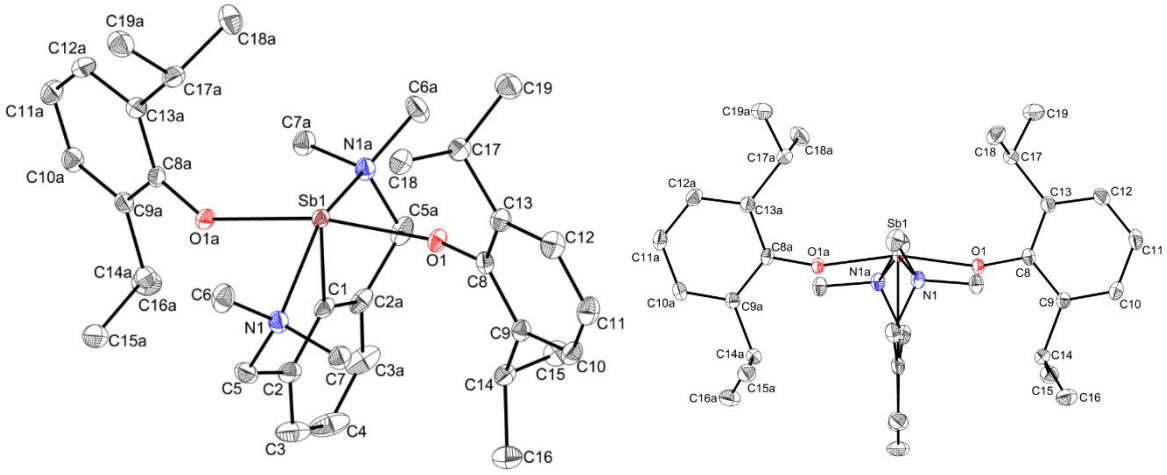

Figure 15. (left) ORTEP representation of the isomer (pR$_{N1}$,pR$_{N1a}$)-**18** with ellipsoids drawn at the 50% probability level [symmetry equivalent atoms (*1–x, y, 1.5–z*) are given by "a"]. (right) View from the plane of the phenyl (*NCN*-aryl) ring. Hydrogen atoms were omitted for clarity.

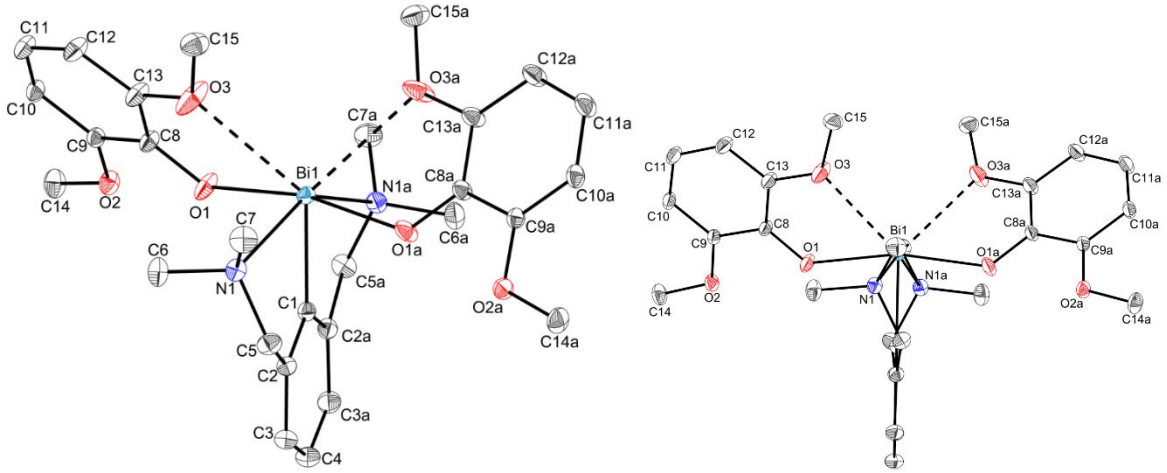

Figure 16. (left) ORTEP representation of the isomer (pS$_{N1}$,pS$_{N1a}$)-**20** with ellipsoids drawn at the 50% probability level [symmetry equivalent atoms (*1–x, y, 0.5–z*) are given by "a"]. (right) View from the plane of the phenyl (*NCN*-aryl) ring. Hydrogen atoms were omitted for clarity.

The molecular structure of **20** exhibits some common trends when compared with the previously reported bismuth(III) bis(aryloxides), R^{1}Bi(OC$_6$H$_3$Me$_2$-2,6)$_2$, and R^{1}Bi(OC$_6$H$_3$^{i}Pr$_2$-2,6)$_2$,[37] namely: *(i)* the nitrogen atoms and oxygen atoms are places mutually in *trans* positions [N1−Bi1−N1a 144.42(3)°; O1−Bi1−O1a 167.26(3)°]; *(ii)* the bismuth atom is strongly coordinated by the *NCN* backbone, as demonstrated by the corresponding Bi−N intramolecular distances [Bi1−N1, Bi1−N1a 2.551(7) Å] in the molecule of **20**. In addition there are also non-covalent interactions between two of the methoxy groups and the bismuth centre [Bi1−O3, Bi−O3a 2.821(9) Å, *cf.* Σr_{vdW}(Bi,O) 4.04 Å[25]].

II.IV. Pnictogen-mediated C−H bond activation. Pnictogen (Sb, Bi) *NCN* pincer complexes with the oxyaryl dianionic ligand $(C_6H_2{}^tBu_2\text{-}3,5\text{-}O\text{-}4)^{2-}$.

R^1SbCl_2 was reacted with 2 equivalents of $KOC_6H_3{}^tBu_2$-2,6, in THF, and a new chartreuse compound was formed, $R^1Sb(C_6H_2{}^tBu_2\text{-}3,5\text{-}O\text{-}4)$ (**21**) [R^1 = 2,6-$(Me_2NCH_2)_2C_6H_3$], similar to $R^1Bi(C_6H_2{}^tBu_2\text{-}3,5\text{-}O\text{-}4)$,[37,38] *inter alia*, by facile C−H bond activation (Scheme 10). The ^1H and $^{13}C\{^1H\}$ NMR spectra of the crude material confirmed the presence of **21** together with the parent phenol, 2,6-$^tBu_2C_6H_3OH$, as the only by-product, in *ca.* 1:1 ratio. Compound **21** was isolated as an air- and moisture-sensitive solid.

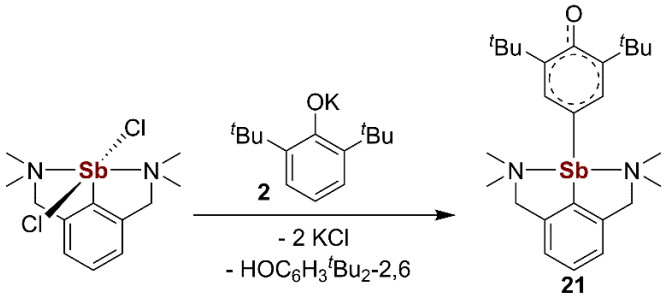

Scheme 10. Synthesis of compound **21**.

The ^1H NMR spectrum of **21** exhibits the characteristic splitting of the R^1 scaffold protons due to a distinct environment induced by the coordinated twisted sidearms, two sharp singlet resonances for the methyl protons and an AB spin system for the diastereotopic methylene protons. A variable temperature ^1H NMR study on **21** in CD_2Cl_2 showed that upon gradually decreasing the temperature, the broad *tert*-butyl singlet resonance reached coalescence at 20 °C ($\Delta G^{\ddagger}$ = 13.5 kcal/mol, calculated with the Eyring equation)[39] and on further cooling becomes broader and it is resolved into two sharp singlet resonances at δ_H 1.31 and 1.04 ppm with $\Delta\delta_H$ 135.95 Hz at −50 °C (Figure 17). Moreover, the broad singlet resonance corresponding to the aromatic protons of the oxyaryl ligand also separated at −50 °C into two sharp singlet resonances at δ_H 7.20 and 6.36 ppm, indicating that rotation is restricted about the Sb−$C_{oxyaryl}$ bond at this temperature.

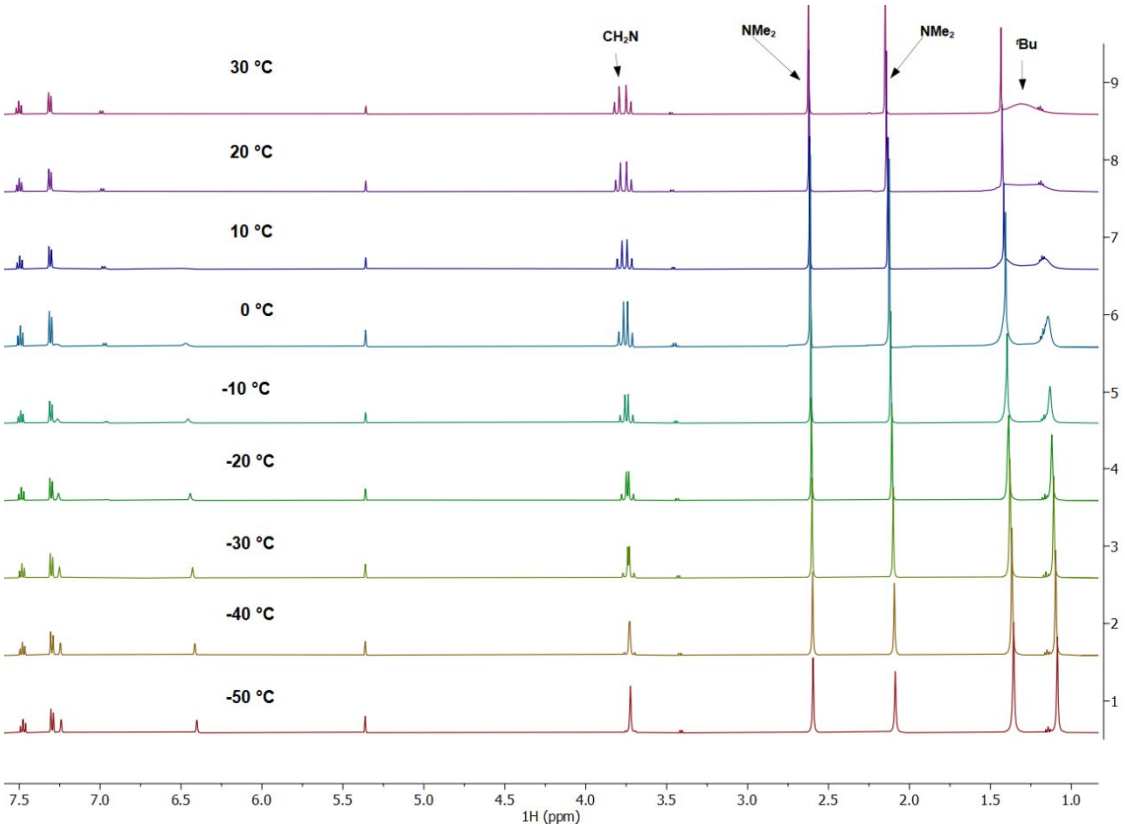

Figure 17. Low variable temperature ^{1}H NMR spectra (CD_2Cl_2, 500.13 MHz) of **21**.

With the aim of further exploring the nature of these pnictogen oxyaryl compounds, the arylpnictogen(III) dichlorides, R^4PnCl_2 [Pn = Sb (**3**), Bi (**4**)], containing the *NCN* ligand scaffold akin to R^1, *i.e.* R^4 = 2,6-(^{i}Pr$_2$NCH$_2$)$_2$C$_6$H$_3$, were reacted with 2 equivalents of KOC$_6$H$_3$^{t}Bu$_2$-2,6 (Scheme 11). Compounds R^4Sb(C$_6$H$_2$^{t}Bu$_2$-3,5-O-4) (**22**) and R^4Bi(C$_6$H$_2$^{t}Bu$_2$-3,5-O-4) (**23**) were immediately formed and after washing the resulted crude materials with hot hexane to remove the undesired 2,6-^{t}Bu$_2$C$_6$H$_3$OH by-product, the title compounds were isolated as orange (**22**) and dark red (**23**) solids stable in inert atmosphere.

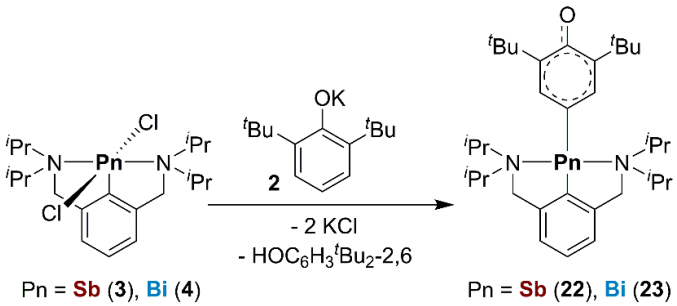

Scheme 11. Syntheses of compounds **22** and **23**.

Solutions of **23** in THF and CD_3CN showed a partial decomposition with a noticeable formation of black precipitate, in just a few hours at room temperature and should be stored at low temperature.

On a par with **21**–**23**, compound $R^2Bi(C_6H_2{}^tBu_2\text{-}3,5\text{-}O\text{-}4)$ (**24**) [R^2 = 2,6-{$MeN(CH_2CH_2)_2NCH_2$}$_2C_6H_3$] was obtained in high yield as a dark red solid, by reacting the parent bismuth(III) dichloride R^2BiCl_2 (**2**) with the potassium aryloxide $KOC_6H_3{}^tBu_2$-2,6 (Scheme 12). The solution behaviour of **24** was also monitored by NMR spectroscopy and the assignment of the resonance signals in the ^1H and $^{13}C\{^1H\}$ NMR spectra was based on the 2D NMR correlation experiments (COSY, HSQC, HMBC and ROESY).

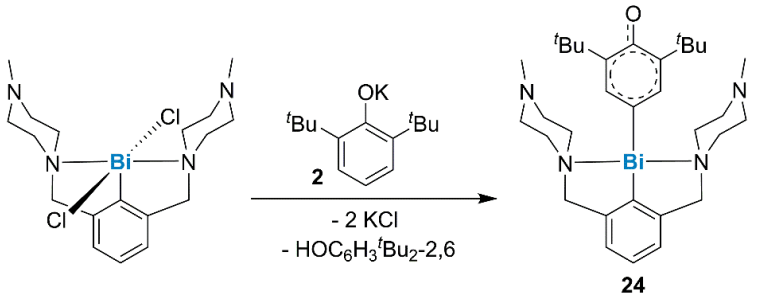

Scheme 12. Synthesis of compound **24**.

A new experiment was designed to elucidate the importance of the *NCN* scaffolds for the stabilisation of the organopnictogen(III) oxyaryl complexes (Scheme 13). Hence, when the arylbismuth(III) dichloride $[2\text{-}(Me_2NCH_2)C_6H_4]BiCl_2$,[40] a hypervalent *10-Bi-4* species,[11] which provides only one pendant arm, was reacted with 2 equivalents of the crowded potassium aryloxide $KOC_6H_3{}^tBu_2$-2,6. different reaction products were obtained, *i.e.* the C–C coupling product 3,3′,5,5′-tetra-*tert*-butyl-4,4′-diphenoquinone (**25**), identified by ^1H and $^{13}C\{^1H\}$ NMR spectroscopy[41] and SCXRD, along with uncharacterised black bismuth material and 2,6-di-*tert*-butylphenol.

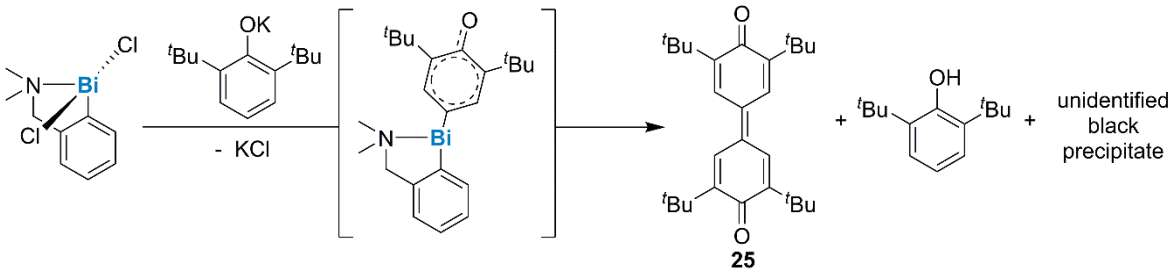

Scheme 13. Formation of C–C coupling products as a result of Bi–O bond homolysis.

The molecular structure of **21** (Figure 18) resembles that of **22** (Figure 19), both compounds feature similar atom connectivity of the oxo ligand $(C_6H_2{}^tBu_2\text{-}3,5\text{-}O\text{-}4)^{2-}$ oriented at right angles with the corresponding *NCN*-aryl ligand [**21**: C1–Sb1–C13 102.28(15)°; **22**: C1–Sb1–C21 98.81(16)°]. The Sb–$C_{(oxyaryl)}$ bond distances in **21** [Sb1–C13

2.098(4) Å] and **22** [Sb1−C21 2.088(2) Å] are equivalent to Sb−C single bonds found in the parent antimony(III) dichloride, R^1SbCl_2, [Sb−C 2.100(9) Å[28]],

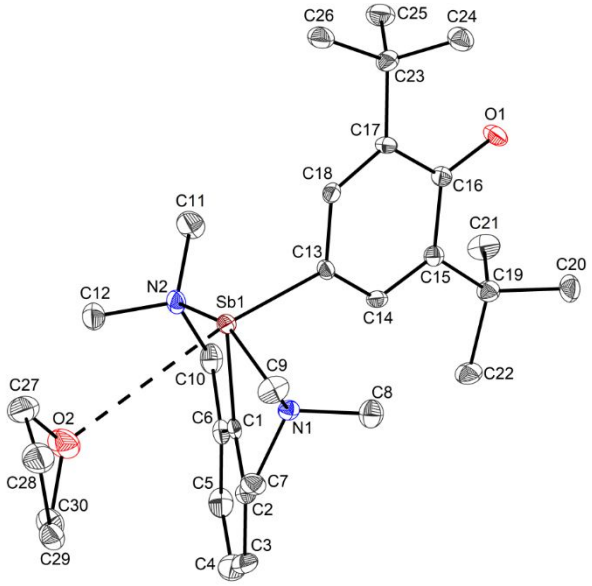

Figure 18. ORTEP representation of the isomer (pR_{N1},pR_{N2})-**21** with ellipsoids drawn at the 50% probability level, present in the crystal of **21**·THF. Hydrogen atoms were omitted for clarity.

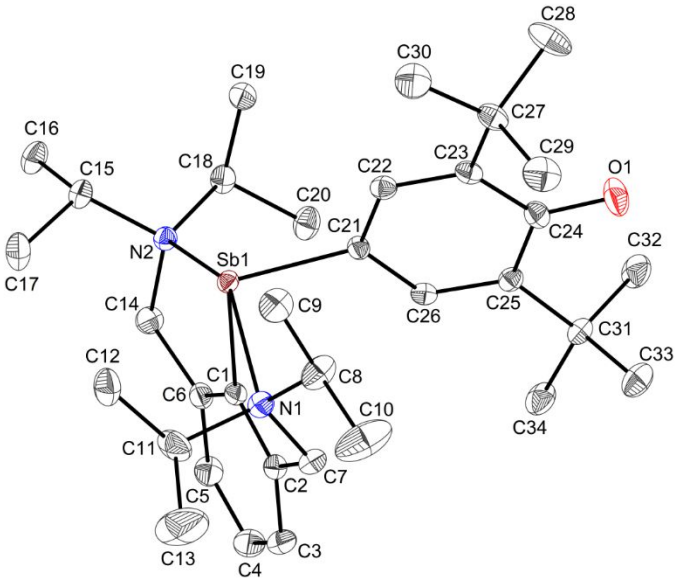

Figure 19. ORTEP representation of the isomer (pS_{N1},pS_{N2})-**22** with ellipsoids drawn at the 50% probability level. Hydrogen atoms were omitted for clarity.

The solid-state molecular structures of **24a** and **24b** (Figure 20) bear a close resemblance to the already reported bismuth(III) oxyaryl complex $R^1Bi(C_6H_2{}^tBu_2$-3,5-O-4) and exhibit similar connectivity of the tridentate *NCN*-aryl backbone, binding the bismuth centres in a *meridional* fashion [**24a**: N1−Bi1−N3 143.53(7)°; **24b**: N5−Bi2−N7 144.55(7)°]. The bismuth-nitrogen bond distances [**24a**: Bi−N 2.569(2), 2.613(2) Å; **24b**:

Bi−N 2.546(2), 2.617(2) Å] are within the sum of the van der Waals radii of the corresponding atoms [*cf.* Σr_{vdW}(Bi,N) 4.20 Å[25]. In compound **24** the two ligand planes defined by the R^2 aryl ligand and the oxyaryl ligand are characterised by a dihedral angle of 83.6° for **24a** and 75.0° for **24b** and if the R^2 is in the arbitrary xy plane, by analogy the oxo ligand in **24a** and **24b** lie in the yz plane so as to efficiently minimise the steric interactions between the aryl ligands.

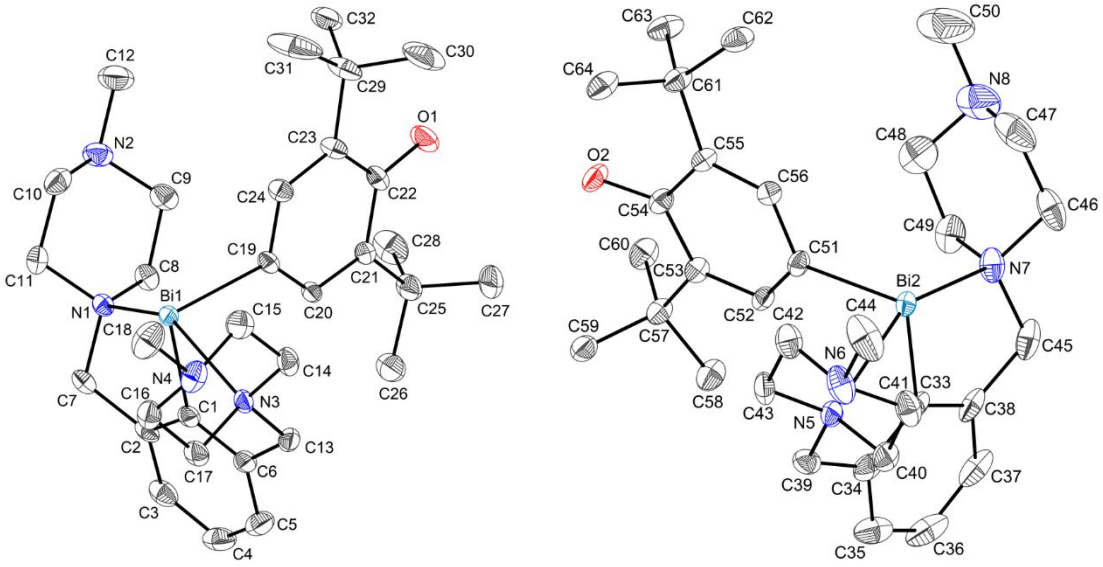

Figure 20. ORTEP representation of the isomers (pS$_{N1}$,pS$_{N3}$)-**24a** (left) and (pR$_{N5}$,pR$_{N7}$)-**24b** (right) with ellipsoids drawn at the 50% probability level. Hydrogen atoms and the THF solvent molecules have been omitted for clarity.

Density functional theory exploration of the proposed mechanism for C−H bond activation.

A plausible mechanism of the C−H activation reaction mechanism has been suggested by Evans and co-workers.[37] It is shown in Scheme 14 below. Evans and co-workers assume, in a preliminary step, the formation of the bis(aryloxide) complex **A**, of which compounds **18−20** are characterised examples. Then, a Bi−O bond homolysis is assumed, following previous suggestions by Hanna *et al.*,[42] to form the **B** and **C** radicals, that subsequently recombine into **D** through the building of a Pn−C_{para} bond. In a final step, **D** eliminates $HOAr^R$ to form the final product **E**, of which compounds **21-24** are characterised examples. This last step might not to be a unimolecular process.

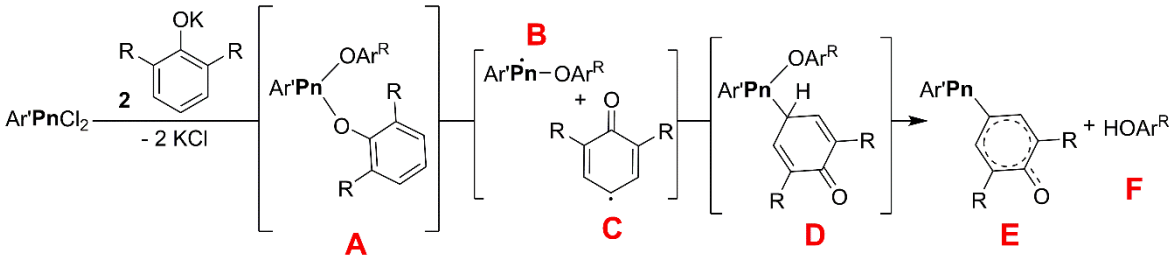

Scheme 14.

In order to shed some light on the realism of this putative mechanism and to understand why all the compounds of type **E** isolated so far correspond to R = ^{t}Bu, we have explored its thermodynamics by DFT calculations in computing the energies of the reactant (**A**), intermediates (**B**, **C**, **D**) and products (**E**, **F**) in Scheme 14. The computed systems correspond to Pn = Sb and Bi, OAr^{R} where R = Me, ^{i}Pr and ^{t}Bu, and Ar′ = 2,6-$(Me_2NCH_2)_2C_6H_3$. Calculations were made with the Gaussian16[43] program at the PBE0/Def2TZVP-D3 level,[44-49] which takes into account the dispersion forces involved in Van der Waals interactions.[49] The geometries of all these species were fully optimised and characterised to be energy minima through vibrational frequency calculations.

III. Conclusions

Four new monoorganoantimony(III) and -bismuth(III) chlorides containing the *NCN* scaffolds 2,6-{$O(CH_2CH_2)_2NCH_2\}_2C_6H_3$ and 2,6-(^{i}Pr$_2$NCH$_2$)$_2$C$_6$H$_3$ were obtained and characterised in solution by multinuclear and 2D NMR spectroscopy. The ^{1}H NMR spectra of compounds [2,6-{$O(CH_2CH_2)_2NCH_2\}_2C_6H_3$]$PnCl_2$ [Pn = Sb (**1**), Bi (**2**)] exhibited similar features, *i.e.* four distinct resonance signals for the morpholinyl equatorial and axial protons, which suggest the existence of intramolecular N→Pn interactions in solution at room temperature. The same observation of N→Pn interactions is maintained for the solution behaviour of [2,6-(^{i}Pr$_2$NCH$_2$)$_2$C$_6$H$_3$]$PnCl_2$ [Pn = Sb (**3**), Bi (**4**)] as revealed by their ^{1}H NMR spectra, whereas the equivalence of the methylene diastereotopic protons on the NMR time scale is indicative of a fast fluxional behaviour which implies *inter alia* the *edge* inversion at the heavier pnictogen centre.

The molecular structures of compounds **1**, **2** and **4** were determined by SCXRD and exhibit in all cases a T-shaped arrangement of the $CPnCl_2$ core strongly coordinated by both pendant arms which resulted in hypervalent *12-Pn-5* species. The *trans* Pn−Cl bond distances in **1**, **2** and **4** are considerably longer than typical Pn−Cl covalent bonds, this behaviour being consistent with the three-centre four-electron theory of the hypervalent bond formation.

Compounds **3** and **4** were found to react with traces of HCl or moisture to form the corresponding zwitterions [2-(^{i}Pr$_2$NCH$_2$)-6-{^{i}Pr$_2$N$^+$(H)CH$_2$}C_6H_3]Sb^-Cl_2(OH) (**5**) and [2-(^{i}Pr$_2$NCH$_2$)-6-{^{i}Pr$_2$N$^+$(H)CH$_2$}C_6H_3]Bi^-Cl_3 (**6**). The protonation of one pendant amine was proved by ^{1}H NMR spectroscopy for **6** and by X-ray diffraction analysis in the case of **5** (established as ionic hypervalent *10-Sb-4* species).

Six new well-defined hypercoordinated organopnictogen(III) bis(arylthiolates) stabilised by various *NCN*-aryl ligands were reported. The solid state structures of $R^1Sb(SC_6H_3Me_2\text{-}2,6)_2$ (**7**) [R^1 = 2,6-(Me$_2$NCH$_2$)$_2$C$_6$H$_3$] and $R^3Sb(SC_6H_3Me_2\text{-}2,6)_2$ (**11**) [R^3 = 2,6-{$O(CH_2CH_2)_2NCH_2\}_2C_6H_3$] exhibit a similar feature, more precisely the potential tridentate *NCN* backbone acts as a *CN*-chelating ligand resulting in an overall distorted *pseudo*-trigonal bipyramidal coordination geometry about antimony atoms (hypervalent *10-Sb-4* species). In contrast, for compounds $R^1Bi(SC_6H_3Me_2\text{-}2,6)_2$ (**8**) and $R^3Bi(SC_6H_3Me_2\text{-}2,6)_2$ (**12**) the *NCN*-pincer behaviour resulted in an overall distorted square pyramidal (*NCN*)BiS_2 core and can be described as hypervalent *12-Bi-5* species.

Compounds **7** and **8** were unstable once exposed to a dry O_2 atmosphere and their decomposition formed the corresponding cyclic oxides *cyclo*-[2,6-$(Me_2NCH_2)_2C_6H_3Pn(\mu$-$O)]_2$ [Pn = Sb (**13**), Bi (**14**)]. The molecular structures of **13** and **14** were determined by SCXRD and revealed as the *anti*-isomers. The oxidative addition of elemental sulfur or selenium to **7** promoted the formation of the S−S coupling by-product ArS−SAr (Ar = $C_6H_3Me_2$-2,6) and gave the heterocyclic species *cyclo*-[2,6-$(Me_2NCH_2)_2C_6H_3Sb(\mu$-E)$]_2$ [E = S (**15**), Se (**16**)]. The solid-state structure of **16** exhibits a close resemblance to **13** and **14** with a slightly asymmetric four-membered Sb_2Se_2 ring and the crystals of **16** contained only the *anti* isomer. A tentative reaction mechanism was proposed based on preliminary data which involved the formation of transient Pn(V) species that are prone to undergo a reductive elimination step, then a fast [2+2] cycloaddition process.

Reaction of $R^3Bi(SC_6H_3Me_2$-2,6$)_2$ (**12**) with a stoichiometric amount of I_2 led to the formation of the diiodide [2,6-$\{O(CH_2CH_2)_2NCH_2\}_2C_6H_3]BiI_2$ (**17**), whereas the use of an excess of I_2 afforded the crystallisation of the first example of a monoorganobismuth(III) adduct with molecular iodine (**17**·0.5$\mathbf{I_2}$), built through halogen bonding as it was established by single-crystal X-ray diffraction.

The synthesis and characterisation of a series of new organopnictogen(III) aryloxides containing the *NCN*-chelating ligand 2,6-$(Me_2NCH_2)_2C_6H_3$ is reported. The solid state structures of $R^1Sb(OC_6H_3{}^iPr_2$-2,6$)_2$ (**18**) revealed the formation of hypervalent *12-Sb-5* species, while in the case of $R^1Bi[OC_6H_3(OMe)_2$-2,6$]_2$ (**20**) the 2,6-$(MeO)_2C_6H_3O$ moieties provide two additional Bi−O interactions, through methoxy groups, resulted in a hepta-coordination environment at the Bi(III) centre. The APCI-HRMS analysis proved that all new reported compounds, **18**−**20**, are susceptible to hydrolysis.

The oxyaryl complexes $R^1Sb(C_6H_2{}^tBu_2$-3,5-O-4) (**21**), [2,6-$(^iPr_2NCH_2)_2C_6H_3]Pn(C_6H_2{}^tBu_2$-3,5-O-4) [Pn = Sb (**22**), Bi (**23**)] and [2,6-$\{MeN(CH_2CH_2)_2NCH_2\}_2C_6H_3]Bi(C_6H_2{}^tBu_2$-3,5-O-4) (**24**) containing the dianionic ligand $(C_6H_2{}^tBu_2$-3,5-O-4$)^{2-}$ were formed by C−H bond activation in a process though to involve the initial step of pnictogen−oxygen bond cleavage. The ^{1}H NMR spectra of **21**−**24** exhibit the characteristic splitting of the *NCN*-aryl scaffolds protons caused by the twisted pincer arms, as a consequence of strong N→Pn interactions which restrict fluxional behaviours in solution usually associated with the *NCN*pincer ligands. Variable low temperature ^{1}H NMR of **21** showed that rotation is restricted about the Sb−$C_{oxyaryl}$ bond at −50 °C and the molecule

is frozen to a structure resembling that found in the solid state. The molecular structures of **21**, **22** and **24** exhibit similar connectivity of the tridentate *NCN*-aryl backbones, binding the pnictogen centre in a *meridional* fashion and being oriented at right angles with the oxyaryl ligand. X-ray crystallography analysis supported that the electronic structure of the dianionic ligands in **21**, **22** and **24** can be characterised as a quinone-like structure.

The reaction of [2-(Me_2NCH_2)C_6H_4]$BiCl_2$ with the potassium phenolate $KOC_6H_3{}^tBu_2$-2,6 did not form the expected bismuth oxyaryl complex, instead the C−C coupling product 3,3′,5,5′-tetra-*tert*-butyl-4,4′-diphenoquinone (**25**) was isolated and identified by ^1H and $^{13}C\{^1H\}$ NMR spectroscopy and by SCXRD along with 2,6-$^tBu_2C_6H_3OH$. These results suggest that the mechanism might involve the formation of radical intermediates and unveil the necessity of a second pendant arm to stabilise the desired pnictogen(oxyaryl) complexes.

DFT calculations on the species (reactant, intermediates and products) involved in the proposed mechanism for the emergence of pnictogen oxyaryl complexes **21**−**24** revealed that the formation of the final complex [2,6-(Me_2NCH_2)$_2C_6H_3$]Pn($C_6H_2R_2$-3,5-O-4) **E** is significantly more favoured in the case of R = ^{t}Bu rather than for R = Me or ^{i}Pr, albeit the system formed of radical intermediates generated after the pnictogen−oxygen bond homolysis is too high in energy and we are presently looking at possible more favourable alternatives.

IV. References

1. C. J. Moulton and B. L. Shaw, *J. Chem. Soc.*, *Dalton Trans.*, 1976, 1020-1024.
2. G. van Koten, K. Timmer, J. G. Noltes and A. L. Speck, *J. Chem. Soc., Chem. Commun.*, 1978, 250-252.
3. J. W. J. Knapen, A. W. van der Made, J. C. de Wilde, P. W. N. M. van Leeuwen, P. Wijkens, D. M. Grove and G. van Koten., *Nature*, 1994, **372**, 659-663;
4. L. A. van de Kuil, D. M. Grove, R. A. Gossage, J. W. Zwikker, L. W. Jenneskens, W. Drenth and G. van Koten, *Organometallics*, 1997, **16**, 4985-4994;
5. A. W. Kleij, R. A. Gossage, R. J. M. Klein Gebbink, N. Brinkmann, E. J. Reijerse, U. Kragl, M. Lutz, A. L. Spek and G. van Koten, *J. Am. Chem. Soc.*, 2000, **122**, 12112-12124.
6. G. van Koten, *Pure Appl. Chem.*, 1989, **61**, 1681-1694.
7. P. P. Power, *Nature*, 2010, **463**, 171-177.
8. D. Martin, M. Soleilhavoup and G. Bertrand, *Chem. Sci.*, 2011, **2**, 389-399.
9. T. Chu and G. I. Nikonov, *Chem. Rev.*, 2018, **118**, 3608-3680.
10. J. I. Musher, *Angew. Chem. Int. Ed. Engl.*, 1969, **8**, 54-68.
11. The *N*–X–L nomenclature system has been previously described: *N* valence shell electrons about a central atom X with L ligands. C. W. Perkins, J. C. Martin, A. J. Arduengo III, W. Lau, A. Alegria and J. K. Kochi, *J. Am. Chem. Soc.*, 1980, **102**, 7753.
12. K. -y. Akiba (Ed.), *Chemistry of Hypervalent Compounds*, Wiley-VCH, New-York, 1999.
13. J. Hicks, P. Vasko, A. Heilmann, J. M. Goicoechea and S. Aldridge, *Angew. Chem. Int. Ed.*, 2020, **59**, 20376-20380.
14. C. Bakewell, A. J. P. White and M. R. Crimmin, *Chem. Sci.*, 2019, **10**, 2452-2458.
15. G. Tan, T. Szilvási, S. Inoue, B. Blom and M. Driess, *J. Am. Chem. Soc.*, 2014, **136**, 9732-9742.
16. X. C. Chen, K. M. Engle, D.-H. Wang and J.-Q. Yu, *Angew. Chem. Int. Ed.*, 2009, **48**, 5094-5115.
17. (a) T. A. Hanna, *Coord. Chem. Rev.*, 2004, **248**, 429-440; (b) C. I. Raț, A. Soran, R. A. Varga and C. Silvestru, *Coord. Chem. Rev.*, 2018, **70**, 233-311.
18. A. Caise, A. E. Crumpton, P. Vasko, J. Hicks, C. McManus, N. H. Rees and S. Aldridge, *Angew. Chem. Int. Ed.*, 2022, **134**, e202114926.
19. L. Copolovici, V. Bojan, C. Silvestru and R. A. Varga, *Acta Crystallogr.*, *Sect. E: Cryst. Commun.*, 2008, **63**, o4570.
20. C. Bibal, S. Mazières, H. Gornitzka and C. Couret, *Polyhedron*, 2002, **21**, 2827-2834.
21. G. Strîmb, A. Pöllnitz, C. I. Raţ and C. Silvestru, *Dalton Trans.*, 2015, **44**, 9927-9942.

22. A. P. Soran, H. J. Breunig, V. Lippolis, M. Arca and C. Silvestru, *Dalton Trans.*, 2009, 77-84.
23. J. Vícha, J. Novotný, S. Komorovsky, M. Straka, M. Kaupp and R. Marek, *Chem. Rev.*, 2020, **120**, 7065-7103.
24. B. Cordero, V. Gómez, A. E. Platero-Prats, M. Revés, J. Echeverría, E. Cremades, F. Barragán and S. Alvarez, *Dalton Trans.*, 2008, 2832-2838.
25. S. Alvarez, *Dalton Trans.*, 2013, **42**, 8617-8636.
26. A. W. Addison, T. N. Rao, J. Reedijk, J. van Rijn and G. C. Verschoor, *J. Chem. Soc., Dalton Trans.*, 1984, 1349-1356.
27. A. P. Soran, C. Silvestru, H. J. Breunig, G. Balázs and J. C. Green, *Organometallics*, 2007, **26**, 1196-1203.
28. D. A. Atwood, A. H. Cowley and J. Ruiz, *Inorg. Chim. Acta*, 1992, **198-200**, 271-274.
29. (a) G. G. Briand and N. Burford, *Adv. Inorg. Chem.*, 2000, **50**, 285-357; (b) L. Agocs, G. G. Briand, N. Burford, M. D. Eelman, N. Aumeerally, D. MacKay, K. N. Robertson, and T. S. Cameron, *Can. J. Chem.*, 2003, **81**, 632-637; (c) S. Moaven, B. T. Watson, S. B. Thompson, V. J. Lyons, D. K. Unruh, D. J. Casadonte, D. Pappas, and A. F. Cazzolino, *Chem. Sci.*, 2020, **11**, 4374-4380.
30. M. Bochmann, X. Song, M. B. Hursthouse and A. Karaulov, *J. Chem. Soc.*, *Dalton Trans.*, 1995, 1649-1652.
31. T. Chatterjee and B. C. Ranu, *RSC Adv.*, 2013, **3**, 10680-10686.
32. L. Dostál, R. Jambor, A. Růžička, M. Erben, R. Jirásko, E. Černošková and J. Holeček, *Organometallics*, 2009, **28**, 2633-2636.
33. A. Fridrichová, T. Svoboda, R. Jambor, Z. Padělkova, A. Růžička, M. Erben, R. Jirásko and L. Dostál, *Organometallics*, 2009, **28**, 5522-5528.
34. L. Dostál, R. Jambor, A. Růžička, R. Jirásko, V. Lochař, L. Beneš and F. de Proft, *Inorg. Chem.*, 2009, **48**, 10495-10497.
35. L. Dostál, R. Jambor, A. Růžička, A. Lyčka, J. Brus and F. de Proft, *Organometallics*, 2008, **27**, 6059-6062.
36. G. R. Desiraju, P. S. Ho, L. Kloo, A. C. Legon, R. Marquardt, P. Metrangolo, P. Politzer, G. Resnati and K. Rissanen, *Pure Appl. Chem.*, 2013, **85**, 1711-1713.
37. I. J. Casely, M. Fang, J. W. Ziller, F. Furche and W. J. Evans, *J. Am. Chem. Soc.*, 2011, **133**, 5244-5247.
38. D. R. Kindra, I. J. Casely, M. E. Fieser, J. W. Ziller, F. Furche and W. J. Evans, *J. Am. Chem. Soc.*, 2013, **135**, 7777-7787.
39. A. Ahmed, R. A. Bragg, J. Clayden, L. W. Lai, C. McCarthy, J. H. Pink, N. Westlund and S. A. Yasin, *Tetrahedron*, 1998, **54**, 13277-13294.
40. C. J. Carmalt, A. H. Cowley, R. D. Culp, R. A. Jones, S. Kamepalli and N. C. Norman, *Inorg. Chem.*, 1997, **36**, 2770-2776.
41. P. Astolfi, M. Panagiotaki and L. Greci, *Eur. J. Org. Chem.*, 2005, 3052-3059.
42. T. A. Hanna, A. L. Rieger, P. H. Rieger and X. Wang, *Inorg. Chem.*, 2002, **41**, 3590-3592.
43. Gaussian 16, Revision C.01, M. J. Frisch, G. W. Trucks, H. B. Schlegel, G. E. Scuseria, M. A. Robb, J. R. Cheeseman, G. Scalmani, V. Barone, G. A. Petersson, H. Nakatsuji, X. Li, M. Caricato, A. V. Marenich, J. Bloino, B. G. Janesko, R. Gomperts, B. Mennucci, H. P. Hratchian, J. V. Ortiz, A. F.

Izmaylov, J. L. Sonnenberg, D. Williams-Young, F. Ding, F. Lipparini, F. Egidi, J. Goings, B. Peng, A. Petrone, T. Henderson, D. Ranasinghe, V. G. Zakrzewski, J. Gao, N. Rega, G. Zheng, W. Liang, M. Hada, M. Ehara, K. Toyota, R. Fukuda, J. Hasegawa, M. Ishida, T. Nakajima, Y. Honda, O. Kitao, H. Nakai, T. Vreven, K. Throssell, J. A. Montgomery, Jr., J. E. Peralta, F. Ogliaro, M. J. Bearpark, J. J. Heyd, E. N. Brothers, K. N. Kudin, V. N. Staroverov, T. A. Keith, R. Kobayashi, J. Normand, K. Raghavachari, A. P. Rendell, J. C. Burant, S. S. Iyengar, J. Tomasi, M. Cossi, J. M. Millam, M. Klene, C. Adamo, R. Cammi, J. W. Ochterski, R. L. Martin, K. Morokuma, O. Farkas, J. B. Foresman, and D. J. Fox, Gaussian, Inc., Wallingford CT, 2016.

44. J. P. Perdew, K. Burke and M. Ernzerhof, *Phys. Rev. Lett.*, 1996, **77**, 3865-3868.
45. J. P. Perdew, K. Burke and M. Ernzerhof, *Phys. Rev. Lett.*, 1997, **78**, 1396.
46. C. Adamo and V. Barone, *J. Chem. Phys.*, 1999, **110**, 6158-6170.
47. A. Schaefer, H. Horn and R. Ahlrichs, *J. Chem. Phys.*, 1992, **97**, 2571-2577
48. A. Schaefer, H. Horn and R. Ahlrichs, *J. Chem. Phys.*, 1994, **100**, 5829-5835.
49. S. Grimme, *J. Comput. Chem.*, 2006, **27**, 1787-1799.

List of relevant articles

1. Organopnictogen(III) bis(arylthiolates) containing *NCN*-aryl pincer ligands: from synthesis and characterization to reactivity
   G. Duneș, A. Soran and C. Silvestru, *Dalton Trans.*, 2022, **51**, 10406-10419. – FI_{2022} = 4.569
   DOI https://doi.org/10.1039/D2DT01436J

2. $[2,6\text{-}\{O(CH_2CH_2)_2NCH_2\}_2C_6H_3]SbCl_2$ - A new pincer ligand-containing organoantimony(III) compound. Molecular structure and supramolecular aspects
   G. Duneș, A. Soran and C. Silvestru, *Rev. Roum. Chim.,* 2022, accepted. – FI_{2022} = 0.278

3. Organoantimony(III) and -bismuth(III) bis(aryloxides)
   G. Duneș and C. Silvestru, *Polyhedron*, 2022, in preparation.

4. The case of antimony(III) and bismuth(III) compounds containing the oxyaryl dianionic ligand $(C_6H_2{}^tBu_2\text{-}3,5\text{-}O\text{-}4)^{2-}$. Structure, reactivity and mechanism.
   G. Duneș, A. Sava, R. Varga, S. Kahlal, J.-Y. Saillard, Y. Sarazin and C. Silvestru, unpublished results.

Conferences

G. Duneș and C. Silvestru, *Organopnictogen(III) bis(arylthiolates) containing NCN-pincer ligands – synthesis, structure and reactivity,* Young Researchers' International Conference on Chemistry and Chemical Engineering (YRICCCE III), 4–5 May, **2021**, Cluj-Napoca, Romania. – oral presentation.

G. Duneș and C. Silvestru*, Aerobic decomposition of new NCN-type pincer organopnictogen(III) bis(arylthiolates),* The 24th Virtual Conference on Organometallic Chemistry (EuCOMC XXIV), 1–3 September, **2021**, Alcala de Henares, Madrid, Spain – oral presentation.